Layer-by-Layer Assembly of Conducting Membranes for Photoelectrochemical Cells

by
Nicole R. Davis

B.S. Chemistry
University of California, Berkeley, 2005

S.M. Chemistry
Massachusetts Institute of Technology, 2009

SUBMITTED TO THE DEPARTMENT OF CHEMISTRY IN PARTIAL FULFILLMENT OF THE REQUIREMENTS FOR THE DEGREE OF

DOCTOR OF PHILOSOPHY IN CHEMISTRY
AT THE
MASSACHUSETTS INSTITUTE OF TECHNOLOGY

SEPTEMBER 2014

Signature redacted

Signature of Author:.. .....
Department of Chemistry
Aug. 8, 2014

Signature redacted

Certified by:... .....
Paula T. Hammond
Professor of Chemical Engineering
Thesis Supervisor

Signature redacted

Accepted by:..... .....
Robert W. Field
Chairman, Departmental Committee on Graduate Students

This doctoral thesis has been examined by a Committee of the Department of Chemistry as follows:

Signature redacted

Professor Timothy M. Swager: ....
Chairman

Signature redacted

Professor Paula T. Hammond: . .....
Thesis Advisor

Signature redacted

Professor Timothy F. Jamison: ....
Dept. of Chemistry

Layer-by-Layer Assembly of Conducting Membranes for Photoelectrochemical Cells

by

Nicole R. Davis

Submitted to the Department of Chemistry
on Aug. 8, 2014 in Partial Fulfillment of the Requirements
for the Degree of Doctor of Philosophy in Chemistry
at the Massachusetts Institute of Technology

ABSTRACT

Spray-assisted layer-by-layer (Spray-LbL) assembly is used to achieve vertical transfer of silicon microwire arrays into an ion-conducting, ultrathin polymer membrane. The choice of LbL platform and the properties of the silicon surface control the film morphology, generating either a conformal coating around each wire or a bridging film across the top of the array. Multilayer transfer printing is used to merge together separately assembled free-standing membrane/microwire assemblies into a single functional film. This technique offers an attractive option relative to traditional materials for microfabrication of Si devices such as solar-driven water splitting systems, capacitors, or electrochemically active electrodes.

Transparent mixed conducting polymer films with conductivity above 0.1 mS/cm are highly desirable for photoelectrochemical cell membrane applications. Mixed conducting polymer composite PEDOT:sPPO was incorporated into LbL films and the composition ratio of the film components was varied to generate a series of films with tunable transparency and electrical and protonic conductivities. The visible light transmission properties are excellent: 1.1 μm thick films with 150 mS/cm electrical conductivity have 80% transmission of light in the visual range. The electronic and ionic conductivities are inversely related, as one can be increased at the expense of the other. The highest ionic conductivity recorded was 4 mS/cm for 4.6 μm thick films with 2 mS/cm electrical conductivity. Electron microscopy was used to provide insight into the effect of film morphology on electrical conductivity, and temperature dependent impededance spectroscopy and ion exchange capacity measurements yielded insight into the ionic conductivity changes.

Thesis Supervisor: Paula T. Hammond
Title: David H. Koch Professor in Engineering

This work is dedicated
to the memory of Officer Sean Collier

Acknowledgements

Many, many thanks my advisor, Prof. Paula Hammond, for welcoming me into her lab, and for all of her guidance and support. I couldn't have asked for a better advisor: Paula is both an excellent scientist and engineer, and an excellent manager and mentor. I always left her office feeling more optimistic and inspired about research than I had been when I entered.

Thanks to my committee members, Prof. Tim Swager and Prof. Tim Jamison, for interesting discussions and research suggestions.

Thanks to my collaborators at Caltech for providing me with silicon microwires, making electrical contact measurements, and for many helpful discussions: Prof. Nate Lewis, Dr. Shane Ardo, Dr. Josh Spurgeon, Dr. Michael Walter, and Heather Audesirk. I would also like to acknowledge all of the participants in the CCI Solar collaboration; I was inspired by their work and learned a great deal from them at the annual meetings.

This work was funded by the NSF under the NSF Center CHE-1305124. Facilities and instruments were provided by the Koch Institute, the CMSE, and the ISN.

I have been lucky to work with many excellent students and postdocs in the Hammond lab. Special thanks go to Dr. David Liu, my comrade-in-arms in the laboratory trenches. We synthesized many, many batches of sPPO together, and we were always bouncing questions and ideas off each other. Special thanks also go to Dr. Junying Liu, with whom I collaborated on the PEDOT:sPPO work. Thanks also to Dr. Nasim Hyder for helpful discussions about spray LbL on microstructured surfaces and for assistance with water contact angle and surface tension measurements. Thanks to Dr. Sung Yeol Kim for advice on electrochemical measurements. I would also like to acknowledge Lucy Fan and Joseph Aboki, two excellent UROP students who worked with me on the spray LbL on microwire arrays and PANI/sPPO LbL film projects. Chad Hunter was another excellent UROP who did some preliminary work on the PEDOT:sPPO tetralayer films. Thanks to Dr. Avni Argun and Dr. Dan Schmidt for passing on knowledge, advice, and ideas for research directions when I first started in the lab. I'd like to thank everyone I overlapped with in the Hammond lab for contributing to the friendly, helpful, and pleasant atmosphere in the lab, it has been a wonderful place to work. Thanks to David, Nasim, Becky, Chibueze, Erik, Julio, Mohi, Nisarg, Jonathon, Abby, Ben, Grinia, Stephen, Po, Noemie, Anasuya, Samantha, Andrew, Lawrence, Bryan, and many others both for helpful research chats and for fun times joking around and chatting in the office and in group meetings.

I would like to acknowledge the professors who first introduced me to chemistry research and encouraged me to pursue and continue my graduate studies: my undergraduate research advisors Prof. Andrew Streitwieser and Prof. Dean Toste, and my master's advisor Prof. Stephen Buchwald. I would especially like to thank the graduate student who I worked with in the Toste lab, Dr. David Gorin, for being an excellent mentor and providing me with a solid foundation in synthetic chemistry techniques.

To the many friends who have supported me throughout this process, I can't imagine finishing grad school without you. Thanks to everyone in my cohort in the chemistry department, especially Julia, Charlene, Dan, Jose, and Jan for sharing encouragement, suffering, and laughter. Thanks to all the roommates who have provided a friendly face and a sympathetic ear to come home to over the years: Pam, Scott, Patrick, Kevin, David, Tony, Jim, and Emma. Thanks to all the climbers who've shared a rope with me these past 5 years for many great adventures, and for pushing me to overcome my limits both in climbing and in the rest of my life: Priam, Josh, Aaron, Becky, Jon, Carrie, Jaclyn, Eugene, Nick, Jim, Ming, Alex, Rosemary, Max, and many others. Thanks are especially due to Lauren, J.D., Jenna, Natalie, Beth, Miriam G., Miriam L. Chris, Carolyn, David, Amy, Melody, and Abhishek for the countless pep talks, hugs, shared meals, and happy memories. And most importantly, thanks to my parents, my brothers, my boyfriend Dave, and his family for all their love and support.

Table of Contents

Chapter 1.

Introduction: Solar Fuels

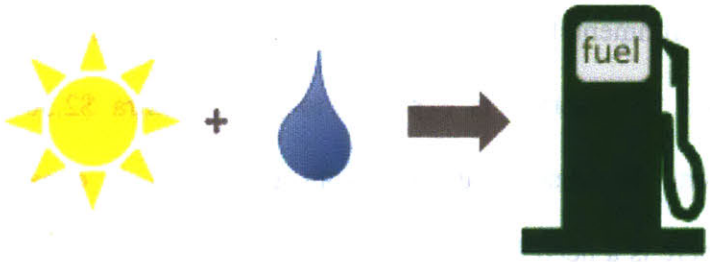

1.1 Motivation and Background

The efficient and economical conversion of solar energy into stored chemical fuels is one of today's chief scientific and technological challenges. Enough solar energy reaches the surface of the earth in one day to power the entire world's energy consumption for more than 20 years. However the temporal and geographical mismatch between solar energy production and demand results in a need for economical, efficient, portable solar energy storage.[1] One of the challenges of integrating renewable sources of energy directly into the current power grid system is the degree of supply uncertainty that they provide. The use of renewables increases the need for reserves and regulation from fuel-based generators, which adds cost and detracts from some of the environmental benefits of using renewables. For example at 15% renewable penetration, the need for reserves is expected to add an extra $2.50 - $5 per MWh of renewable generation.[2] Because regulation from generators is expensive and produces greenhouse gases, there is a need for economical and efficient solar energy storage. Artificial photosynthesis, the use of solar energy to directly generate H_2 or other fuels, is a huge area of research focused on filling this need.[1, 3]

An economical and non-greenhouse-gas-producing source of hydrogen is also needed to enable the infrastructure required for hydrogen fuel cell vehicles. Consumer-level hydrogen fuel cell electric vehicles are coming to market in California in 2015.[4] California currently has 9 hydrogen filling stations in operation, only one of which uses solar powered electrolysis to produce hydrogen on site.[5] The majority of the others rely on natural gas reformation, which is more expensive than gasoline (currently $8–10 per gallon of gasoline equivalent in CA) and produces CO_2 (Figure 1.1).

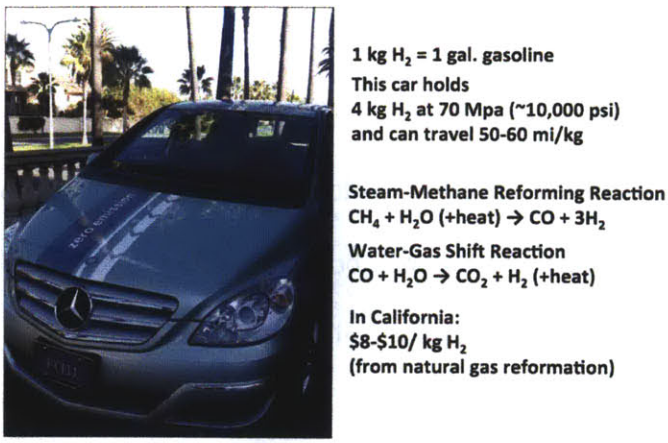

Figure 1.1. Mercedes-Benz B-Class F-CELL hydrogen fuel cell electric vehicle. These cars have been in operation in Europe and the US since 2010, and similar versions will be available to consumers in CA in 2015.

Solar powered water electrolysis could provide energy storage and a source of carbon-free hydrogen. The average American home uses 20 kW-h of electricity per day: this amount of electricity could be supplied by splitting 5.5 L of water per day.[6] To put this number in context, a standard toilet flush uses 6 L of water, and the average American family of four uses 1500 L of water per day.[7]

Water Splitting

$$2H_2O \longrightarrow 2H_2 + O_2$$

$$4H^+ + 4e^- \longrightarrow 2H2$$

$$2H_2O \longrightarrow O_2 + 4e^-$$

Figure 1.2. Equation for water-splitting.

Jaramillo et al. performed an extensive study of the technoeconomics of photoelectrochemical H_2 to determine if this method of producing hydrogen could be cost competitive with natural gas (target $2–4/ gallon of gasoline equivalent).[8] They determined

that efficiency of the process is the biggest cost driver,[8a] and that cost effective H_2 could be produced using the current state-of-the-art materials.[8b]

Nocera et al. published an artificial leaf device that was 2.5% efficient at 1 sun.[1] However, this device did not contain a membrane, resulting in several disadvantages. In this device proton transport occurred through the electrolyte around the sides of the device, which is a relatively long distance for ion transport, and thus resulted in substantial Ohmic losses. Additionally, without a membrane to provide gas separation, a dangerous mix of gases could be produced (the safety limit for hydrogen in oxygen is 4%). Also, in order to separate out the desired hydrogen product, various engineering solutions would need to be employed, thus adding to the cost. Developing a membrane for a wireless, membrane-supported artificial photosynthesis device is the goal of the work described herein.

1.2 Center for Chemical Innovation Device Design

This project was designed as part of the National Science Foundation Center for Chemical Innovation on Solar Fuels, which was composed of a large group of collaborating scientists from across the US who were each working on separate aspects of a proposed solar-powered water-splitting device.[9] The proposed device design (Figure 1.3) involves microstructured semiconductor photoelectrodes in order to orthogonalize the directions of light absorption and charge transport.[10] This allows a long distance through which to absorb light because inorganic materials typically have lower absorption coefficients than organic materials. The charges generated can travel in the radial direction, allowing the use of cheaper materials with lower charge diffusion lengths than the more expensive single crystalline materials.[10] The cathode is envisioned to be Si microwires, and the anode would be a

semiconductor material with a complimentary band gap to Si, such that more of the solar spectrum can be absorbed and the additive voltage from the band gaps will be enough to drive water splitting without an external voltage source (which requires 1.23 V plus overpotential, which is dependent on catalyst choice). Oxygen and hydrogen evolving catalysts will be coated on or attached to the photoelectrode wires. The device is supported by a multifunctional membrane. The ideal membrane would be mixed conducting, have low permeability to H_2 and O_2, be optically transparent and water stable. Each of these properties will be discussed in detail below.

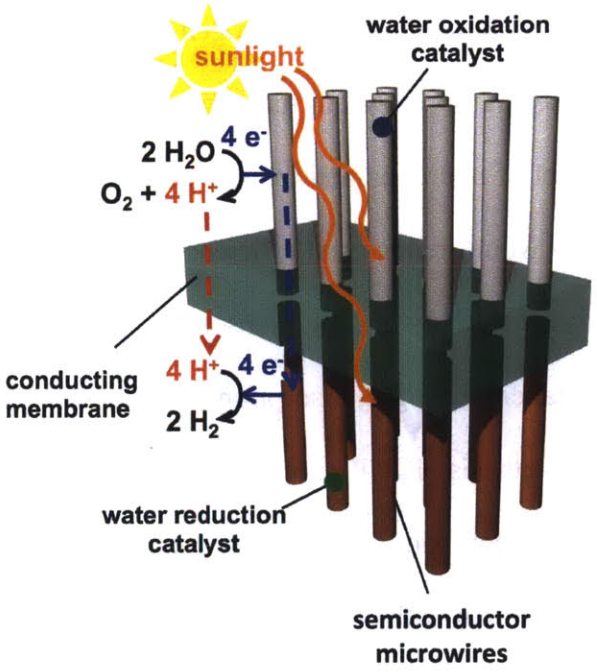

Figure 1.3. Proposed wireless solar-powered water-splitting device design.

The membrane in the device is required to be mixed conducting, essentially replacing both the wires and the salt bridge of a typical electrochemical cell. With the membrane providing electrical conductivity, the microwires of the anode and cathode need not be aligned. The membrane must be protonically conducting because a pH gradient will be

formed as protons are produced at the anode and reduced to hydrogen at the cathode. Whichever conductivity is lower will set the ohmic losses for the device, so ideally the ionic and electrical conductivities would be close to equal. Modeling studies have suggested a target minimum conductivity of 8 mS/cm for a 40 μm thick membrane based on allowing less than 1% voltage losses and a current density of 20 mA cm^{-2} (this current density is based on a solar photon flux of 4 mmol s^{-1} m^{-2}).[11] More extensive modeling studies taking into account various device architectures have suggested an even lower minimum conductivity target of 0.1 mS/cm for membranes less than 10 μm thick.[12]

Another membrane requirement is low hydrogen and oxygen permeability, so that the membrane can act as a separator between the product gases. If the membrane is too permeable, a dangerous level of hydrogen and oxygen mixing can occur, and this would also provide a back current that would reduce the efficiency of the device. There is a trade–off between permeability and conductivity and light absorption. Thicker films will have less gas crossover, but higher resistance and light absorption. A recent modeling study by the Joint Center for Artificial Photosynthesis (JCAP) examined the tradeoff between gas permeability and conductivity and the effects on device performance.[13] They found that the ionic conductivity can drop to 1.2 mS/cm with only a 5% loss in net H_2 collected compared to using a Nafion membrane with ionic conductivity of 100 mS/cm.[13] However if the gas permeability droped by an order of magnitude compared to Nafion permeability (H_2 permeation coefficient of $1.6x10^{-11}$ mol $cm^{-1}s^{-1}bar^{-1}$ and O_2 coefficient of $1.05x10^{-11}$ mol $cm^{-1}s^{-1}bar^{-1}$), the net H_2 collected increased by 63.5%.[13] Thus the device efficiency is much more sensitive to gas crossover than to ionic conductivity.

Additionally, the membrane must be minimally absorbing in the visible range, so that the wavelengths of light that are too long to be absorbed by the photoelectrode with the higher band gap can pass through the membrane to be absorbed by the material with the lower bandgap. The membrane also has mechanical strength and water stability requirements to support the wires while immersed in water. Additionally, the membrane should be easy to fabricate, in order for the ultimate device to be economical.

There are no current materials that can fulfill all of the requirements of this multifunctional membrane. The goal of this work was to develop new materials that can fill this gap. Another goal was to develop microfabrication techniques to generate structures like the proposed device. Ideally the technique used would be modular, so that the anode and cathode microwire/membrane assemblies could be fabricated separately, and to provide design flexibility as the ultimate materials and components are areas of active research and as such, subject to change.

1.3 Choice of Materials and Techniques

If we were to choose two random polymers off the shelf and attempt to generate a blend, we would have little control over the mixing and morphology of the polymers at the nanoscale. Hence for our goal of combining an electrically conducting polymer and an ionically conducting polymer into a mixed conducting film, we chose to use layer-by-layer (LbL) assembly because it allowed us to avoid the limitations of traditional polymer blends. LbL is a versatile water-based thin-film fabrication technique that utilizes alternating layers of complimentary functionalized materials, such as oppositely charged polymers, or hydrogen-bond donor- and accepter-containing polymers.[14] A variety of nanomaterials can be

incorporated in addition to polymers such as carbon nanotubes,[15] polymer nanofibers,[16] and inorganic nanoparticles,[17] and nearly any substrate can be used. A typical LbL process involves immersing a negatively charged substrate into a dilute aqueous solution of polycation, followed by a series of rinse steps to remove excess polymer, leaving enough polymer behind to reverse the surface charge. Then the substrate is immersed in a polyanion solution, again followed by rinse steps (Figure 1.4). This process constitutes one bilayer (BL) and can be repeated to generate films of the desired thickness. LbL films are not highly stratified, as there is interpenetration between the layers, so LbL can create materials that are essentially nanoscale blends. Other advantages of the LbL technique for this application are a high degree of composition control, adaptable aqueous processing conditions, and nanometer scale thickness control. Several platforms can be used for LbL assembly, including dipping, spraying,[18] spin-assisted assembly,[19] and roll-to-roll processing.

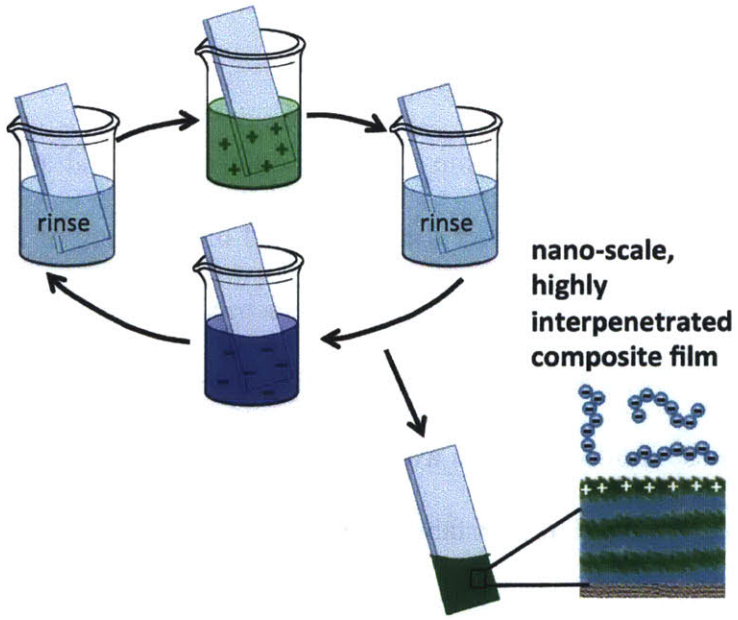

Figure 1.4. Illustration of the layer-by-layer assembly process.

For the ion-conducting component of our membranes we chose to use sulfonated poly(2,6-dimethyl-1,4-phenylene oxide) (sPPO), which has an extremely high ionic conductivity of 400–600 mS/cm with a degree of sulfonation above 80%. However, sPPO is water soluble, so it needs to be stabilized in order to be used as a membrane in water. Using sPPO in an LbL film introduces electrostatic cross-links that stabilize the film in water. An LbL system composed of sPPO and poly(dimethyldiallylammonium chloride) (PDAC) was shown to have ionic conductivity of up to 70 mS/cm when fully humidified.[20] PDAC/sPPO was also shown to have low permeability to small molecules such as methanol. Using PDAC/sPPO coated Nafion as the proton exchange membrane in a direct methanol fuel cell resulted in an increased power output of 50% due to the decreased fuel cross-over.[20] Thus we hypothesized that the use of these polymers would help regulate H_2 and O_2 crossover as well.

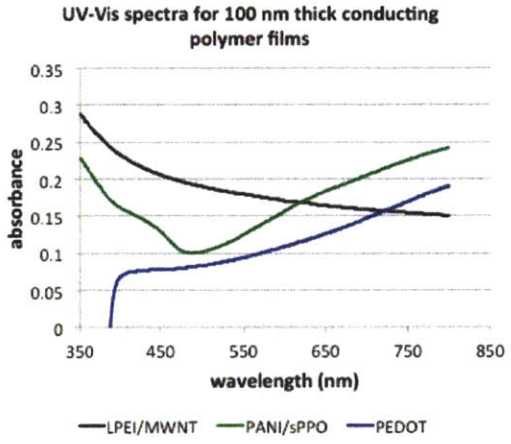

Figure 1.5. UV-Vis absorption spectra for 100 nm thick conducting polymer films of spin cast PEDOT:PSS, LbL assembled PANI/sPPO, and LbL assembled LPEI/MWNT (linear polyethylene imine/ amine functionalized multi-walled carbon nanotubes).

For the electrically conducting component we initially chose to work with polyaniline (PANI), which is cationic when in its conductive emeraldine salt phase, and amine-

functionalized carbon nanotubes (MWNTs). However these materials are very strongly absorbing in the visual range, and so they were abandoned in favor of poly(3,4-ethylenedioxythiophene) (PEDOT) which is one of the most transparent and stable conducting polymers.[21]

1.4 Thesis Overview

The objectives of this thesis were to develop materials and fabrication methods that could be used to generate transparent mixed conducting membranes and to integrate them with microstructured electrodes for photoelectrochemical cells.

Chapter 2 discusses fabrication methods to incorporate LbL films with silicon microwires in a controlled fashion. The factors that determine the location of film formation on microwire arrays are identified. The LbL multilayer transfer printing technique is adapted to combining separate membranes in order to fabricate modular structures. A proof-of-principle model device structure containing two silicon wire arrays supported in a proton conducting membrane is assembled.

Chapter 3 discusses new transparent mixed conducting materials with tunable properties. The morphology of these materials is investigated to understand its effect on electrical conductivity. Also described is the use of impedance spectroscopy to separate the ionic and electrical conductivities, as well as experiments to understand the cause of ionic conductivity improvements.

Appendix A contains data on the early efforts towards mixed conducting LbL films of sPPO with PANI and MWNTs.

Appendix B illustrates preliminary efforts to combine the mixed conducting materials of Ch. 3 with the fabrication methods of Ch. 2.

1.5 References

1. Bensaid, S.; Centi, G.; Garrone, E.; Perathoner, S.; Saracco, G., Towards Artificial Leaves for Solar Hydrogen and Fuels from Carbon Dioxide. *ChemSusChem* **2012,** *5*, 500-521.
2. EnerNex Corporation, Eastern Wind Integration and Transmission Study. **2010**.
3. McKone, J. R.; Lewis, N. S.; Gray, H. B., Will Solar-Driven Water-Splitting Devices See the Light of Day? *Chem. Mater.* **2014,** *26*, 407-414.
4. Toyota http://www.toyota.com/fuelcell/.
5. California Fuel Cell Partnership http://cafcp.org/stations/emeryville_-_ac_transit.
6. Nocera, D. G., Chemistry of Personalized Solar Energy. *Inorganic Chemistry* **2009,** *48* (21), 10001-10017.
7. EPA http://www.epa.gov/WaterSense/pubs/indoor.html.
8. (a) Pinaud, B. A.; Benck, J. D.; Seitz, L. C.; Forman, A. J.; Chen, Z.; Deutsch, T. G.; James, B. D.; Baum, K. N.; Baum, G. N.; Ardo, S.; Wang, H.; Millere, E.; Jaramillo, T. F., Technical and economic feasibility of centralized facilities for solar hydrogen production via photocatalysis and photoelectrochemistry. *Energy Environ. Sci.* **2013,** *6*, 1983; (b) Seitz, L. C.; Chen, Z.; Forman, A. J.; Pinaud, B. A.; Benck, J. D.; Jaramillo, T. F., Modeling Practical Performance Limits of Photoelectrochemical Water Splitting Based on the Current State of Materials Research. *ChemSusChem* **2014,** *7* (5), 1372-1385.
9. http://www.ccisolar.caltech.edu.
10. Kayes, B. M.; Atwater, H. A.; Lewis, N. S., Comparison of the device physics principles of planar and radial p-n junction nanorod solar cells. *Journal of Applied Physics* **2005,** *97*, 114302.
11. McFarlane, S. L.; Day, B. A.; McEleney, K.; Freund, M. S.; Lewis, N. S., Designing electronic/ionic conducting membranes for artificial photosynthesis. *Energy & Environmental Science* **2011,** *4*, 1700-1703.
12. Haussener, S.; Xiang, C.; Spurgeon, J. M.; Ardo, S.; Lewis, N. S.; Weber, A. Z., Modeling, simulation, and design criteria for photoelectrochemical water-splitting systems. *Energy & Environmental Science* **2012,** *5*, 9922-9935.
13. Berger, A.; Segalmanab, R. A.; Newman, J., Material requirements for membrane separators in a water-splitting photoelectrochemical cell. *Energy Environ. Sci.* **2014,** *7*, 1468.
14. Decher, G., Fuzzy Nanoassemblies: Toward Layered Polymeric Multicomposites. *Science* **1997,** *277*, 1232.
15. Lee, S. W.; Kim, B. S.; Chen, S.; Shao-Horn, Y.; Hammond, P. T., Layer-by-Layer Assembly of All Carbon Nanotube Ultrathin Films for Electrochemical Applications. *Journal of the American Chemical Society* **2009,** *131* (2), 671-679.
16. Hyder, M. N.; Lee, S. W.; Cebeci, F. C.; Schmidt, D. J.; Shao-Horn, Y.; Hammond, P. T., Layer-by-Layer Assembled Polyaniline Nanofiber/Multiwall Carbon Nanotube Thin Film Electrodes for High-Power and High-Energy Storage Applications. *Acs Nano* **2011,** *5* (11), 8552-8561.

17. Kurt, P.; Banerjee, D.; Cohen, R. E.; Rubner, M. F., Structural color via layer-by-layer deposition: layered nanoparticle arrays with near-UV and visible reflectivity bands. *Journal of Materials Chemistry* **2009,** *19* (47), 8920-8927.
18. (a) Krogman, K. C.; Cohen, R. E.; Hammond, P. T.; Rubner, M. F.; Wang, B. N., Industrial-scale spray layer-by-layer assembly for production of biomimetic photonic systems. *Bioinspiration & Biomimetics* **2013,** *8* (4); (b) Krogman, K. C.; Lowery, J. L.; Zacharia, N. S.; Rutledge, G. C.; Hammond, P. T., Spraying asymmetry into functional membranes layer-by-layer. *Nature Materials* **2009,** *8* (6), 512-518; (c) Krogman, K. C.; Zacharia, N. S.; Schroeder, S.; Hammond, P. T., Automated Process for Improved Uniformity and Versatility of Layer-by-Layer Deposition. *Langmuir* **2007,** *23* (6), 3137-3141.
19. Cho, J.; Char, K.; Hong, J. D.; Lee, K. B., Fabrication of Highly Ordered Multilayer Films Using a Spin Self-Assembly Method. *Advanced Materials* **2001,** *13* (14), 1076-1078.
20. (a) Argun, A. A.; Ashcraft, J. N.; Hammond, P. T., Highly Conductive, Methanol Resistant Polyelectrolyte Multilayers. *Advanced Materials* **2008,** *20*, 1539-1543; (b) Ashcraft, J. N.; Argun, A. A.; Hammond, P. T., Structure-property studies of highly conductive layer-by-layer assembled membranes for fuel cell PEM applications. *Journal of Materials Chemistry* **2010,** *20*, 6250-6257.
21. Groenendaal, L.; Jonas, F.; Freitag, D.; Pielartzik, H.; Reynolds, J. R., Poly(3,4-ethylenedioxythiophene) and Its Derivatives: Past, Present, and Future. *Adv. Mater.* **2000,** *12*, 481.

Chapter 2.

Microfabrication of Ion-Conducting Membrane-Electrode Assemblies by Spray Layer-by-Layer Assembly

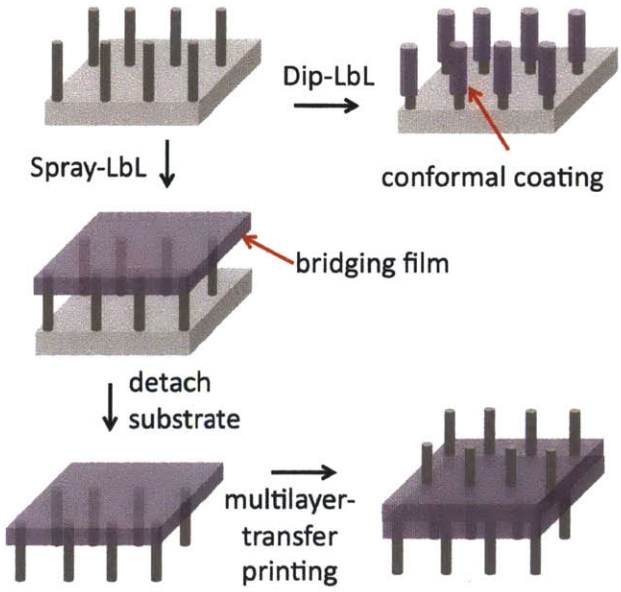

ABSTRACT: Spray-assisted layer-by-layer (Spray-LbL) assembly is used to achieve vertical transfer of silicon microwire arrays into an ion-conducting, ultrathin polymer membrane. The choice of LbL platform and the properties of the silicon surface control the film morphology, generating either a conformal coating around each wire or a bridging film across the top of the array. Multilayer transfer printing is used to merge together separately assembled free-standing membrane/microwire assemblies into a single functional film. This technique offers an attractive option relative to traditional materials for microfabrication of Si devices such as solar-driven water splitting systems, capacitors, or electrochemically active electrodes.

2. 1 Introduction

Arrays of vertically aligned semiconductor micro- or nano-wires are important components in a variety of devices such as solar cells,[1] artificial photosynthesis systems,[2] thermoelectric modules,[3] and field-effect transistors.[4] Most of these arrays have been generated either by etching or by chemical vapor deposition processes on bulk semiconductor wafers; however, to be used in active devices, it is necessary to manipulate these arrays and embed them in other matrices with characteristics such as ionic conductivity, electronic conductivity, specific membrane properties, and/or a range of mechanical properties. Additionally, the wire arrays must be removed from the substrate to take maximum advantage of their unique optical and electronic properties.[5] Furthermore, such removal allows for the reuse of the original substrate as an epitaxial growth support for producing additional wire arrays.[6] The embedding of semiconductor wire arrays into polymers can create flexible electronics, which in turn would enable the use of such systems in new applications such as wearable electronics[7] and the opportunity to exploit inexpensive processing techniques.[6]

Vertically oriented micro- and nano-wire semiconductor arrays have been embedded in polymers such as polydimethylsiloxane (PDMS),[6] poly(methyl methacrylate) (PMMA),[5] and paralene,[3a] but few systems have utilized functional polymers as the supporting medium.[2b]

We were intrigued by the properties that might arise from the combination of semiconductor microwire arrays with functionalized polymers. We were further inspired to develop such a composite material by a proposed device structure consisting of two sets of microwires supported in an ordered, vertical arrangement on opposite sides of an ionically and electronically conducting polymer membrane. Such a device would require a method of transferring the wires into the membrane and would ideally be modular, such that both sets of wires could be grown separately. In order to investigate the fabrication of a model device, we chose to use silicon microwires grown by a VLS process (vapor-liquid-solid mechanism of chemical vapor deposition) from a patterned silicon wafer, with dimensions that have been optimized for use in photovoltaic[8] and photoelectrochemical devices.[2b]

To deposit the functionalized polymer onto the wire array, we selected layer-by-layer (LbL) assembly. LbL is a versatile fabrication technique that involves sequential adsorption of complementary functionalized materials, such as oppositely charged polyelectrolytes, from aqueous solutions.[9] The LbL approach affords the ability to generate thin-film composites that are effectively nanoscale blends. Herein we focus on the use of an automated spray layer-by-layer (Spray-LbL)[10] technique, which has the advantage of dramatically reducing assembly time compared to the more traditional method of dipping the substrate with its nascent composite film into the polyelectrolyte solution (Dip-LbL). Dip-LbL films have been shown to conformally coat complex substrates, however, Spray-LbL has been used to modulate the

manner by which multilayer thin films coat membranes and other porous surfaces: either conformally coating or bridging pores depending on the conditions used.[10b]

Herein we describe the use of layer-by-layer (LbL) assembly to achieve the transfer of vertically oriented silicon microwire arrays into an ion-conducting, ultrathin polymer membrane. We have exploited the nature of film formation on highly structured surfaces to create microstructures that are appropriate for device assembly with microwires. Two ion-conductive LbL systems were used as model functional membranes to explore the suitability of the Spray-LbL method for embedding and transfer of silicon microwire arrays. We chose to look at both a weak (LPEI/PAA)[11] and a strong (PDAC/sPPO)[12] polyelectrolyte pair because they exhibit different assembly behaviors, as described in detail in previous work.

The ability to control the thickness of the film with nano-scale accuracy, to fine tune its composition along the *z*-direction, and to limit film formation to specific regions of the wire array are attractive features of the LbL method that distinguish it from the use of bulk polymers. Another advantage over bulk polymer methods is that polymer-on-polymer stamping[13] and multilayer transfer[14] techniques have been developed to print and manipulate LbL films post-assembly, and these techniques can be used to create complex micro-patterns in 2-D.[15] Our current work extends the use of multilayer transfer to 3 dimensional structures, allowing LbL films to be used as glue to assemble modular structures while still retaining the conductive properties of the films.

2.2 Materials and Methods

2.2.1 Polymer solutions: PPO (MW = 23,000), PDAC (MW = 240,000), and PEO (MW = 4,000,000) were obtained from Sigma-Aldrich. LPEI (MW = 250,000) and PAA (MW =

90,000) were obtained from Polysciences. sPPO was synthesized as reported previously.[12a] The concentration of the PDAC and sPPO polymer solutions was 10 mM (based on repeat unit MW). The pH of these polymer solutions was adjusted to pH 2 by the addition of HCl, and the ionic strength was adjusted by addition of NaCl. Rinse solutions were adjusted to the same pH and ionic strength as the polymer solutions. For the LPEI/PAA films, the polymer solutions were 20 mM in concentration and were adjusted to pH 4.75 with HCl or NaOH, and the rinse solutions were deionized water with no pH adjustment. Surface tension of the polymer solutions was measured using drop shape image analysis.

2.2.2 Silicon Wire Growth: Si microwire arrays were patterned and grown as described previously.[6] Wire arrays were grown from Si(111) wafers patterned with regularly spaced arrays of catalyst islands. These were produced by photolithographically patterning photoresist on an oxide covered Si wafer, etching away the oxide layer by exposing the wafer for 4 min to buffered HF, followed by thermal evaporation of 300 nm of Cu, and lift-off of the resist. After application of catalyst, samples were annealed in a tube furnace at 900–1000 °C for 20 min under 1 atm of H_2 at a flow rate of 1000 sccm, followed by wire growth at the same temperature under 1 atm of H_2 and $SiCl_4$, at flow rates of 1000 and 20 sccm, respectively. Time allowed for wire growth controlled wire height. Upon removal from the growth reactor, the wire surfaces became oxidized. Total array areas were ~ 6 cm^2.

Wire Diameter (μm)	Center to Center Pitch (μm)	Array Geometry	Wire Height (μm)
0.7	2.5	square	140-150
1.8	7	square	25-100
7.5	20	hexagonal	40

2.2.3 Silicon Substrate Treatment: All planar and microwire array Si substrates were cleaned to remove contaminants, native oxide, and Cu catalyst by repeating this series of steps twice: **1.** 10 s in 10% aq. HF, **2.** Water rinse, N_2 blow dry, **3.** 20 min at 70 °C in 6:1:1 by volume water: conc. HCl: 30% H_2O_2, **4.** Water rinse, N_2 blow dry. For the Si-H substrates, the surface was treated with 10% aqueous HF for 15 s, rinsed with water and dried immediately before use. For the Si-OH substrates the sample was placed in an O_2 plasma cleaner for 4 min on high power prior to use. For the Si-$(CH_2)_2(CF_2)_5CF_3$ substrates the samples were incubated with 1 mL of trichloro(1H,1H,2H,2H-perfluorooctyl)silane in a vacuum dessicator, active vacuum was applied for 5 min, then the dessicator was sealed overnight. The substrates were washed with hexanes and acetone before use.

2.2.4 Dip layer-by-layer assembly: A programmable ZEISS DS50 slide stainer was used to deposit films. To construct LbL films, substrates were immersed in a 10 mM PDAC solution for 15 min, then in a series of three water rinse baths for 2 min each, followed by immersion into a 10 mM sPPO solution for 15 min, then into a series of three water rinse baths for 2 min each. This process produced one bilayer (BL). The process was repeated until films had the desired thickness.

2.2.5 Spray layer-by-layer assembly: A programmable sprayer was used to deposit films.[28] Substrates were held in a vertical orientation 7 in. from the spray outlets and rotated at 20 rpm while being sprayed at 22 psi for the specified time (1–10 s) at rate of 0.25–0.3 mL/s. One bilayer (BL) was produced via this series of spray steps: 1–10 s polycation solution, drain time equal to spray time, 5 s rinse spray, 5 s drain, 1–10 s polyanion solution (equal time period as the polycation), drain, 5 s rinse, 5 s drain. This process was repeated until the desired film thickness was attained.

2.2.6 LbL film merging: LbL films with oppositely charged top layers, one ending in PDAC, the other ending in sPPO, were enclosed in a humidity chamber for 30 min at 90% relative humidity (RH). The films were then placed in contact and subjected to pressure (clamped with a binder clip or placed under a glass slide with a 25 g weight on top), and were enclosed in a humidity chamber at 90% RH for 1-48 h. Films were also merged while wet by placing a drop of either a polymer solution (same solution as used for film assembly) or a 0.5 M NaCl solution on the film surface, clamping them together with a binder clip, followed by drying in an oven at 50°C for 2 h. The pressure (binder clip or weight) was removed after drying and the films remained stuck together even when subjected to attempted manual separation.

2.2.7 Film Thickness: Thickness measurements were made by scoring films on flat substrates (glass or silicon) with a razor blade. The step height between the film and substrate was then measured with a Dektak 150 surface profiler.

2.2.8 Microscopy: SEM images were obtained using a JEOL JSM-6060 SEM instrument on Au-coated samples. Dimensions in the images were measured using ImageJ to determine the number of pixels per micron. Cross-sectional images were obtained by freezing samples in liquid nitrogen prior to fracturing them.

2.2.9 Ionic conductivity: Conductivity values were determined by impedance spectroscopy (Solartron 1260 impedance analyzer), by sweeping the frequency from 100 kHz to 0.1 Hz, with a sinusoidal voltage amplitude of 50 mV. Samples were enclosed in a humidity chamber and were allowed to equilibrate for 30 min prior to the measurements. Impedance spectra were modeled using an equivalent circuit consisting of a resistor (representing parasitic lead resistance) in series with the parallel combination of a constant phase element and a resistor (representing bulk electrolyte polarization and resistance to ion motion, respectively).[11]

2.3 Results and Discussion

The morphology of LbL coatings can be controlled on the surfaces of micron-scale wire arrays, as illustrated in the schematic (Figure 2.1). When coating high aspect-ratio arrays with LbL films, conformal coatings can be formed around the surfaces of the wires, or bridging films can be generated across the tops of the wires. Controlling the location of film formation on the wire arrays is advantageous, as it allows customization of placement of the film for the desired application. For example, if one wanted to coat the microarray with capacitive elements, carbon nanotubes, electroactive, photoactive or other components, it would be possible to do so with a great deal of control. To achieve a conducting interface between microwire arrays, one can generate active or inert LbL films that bridge across the base of the arrays.

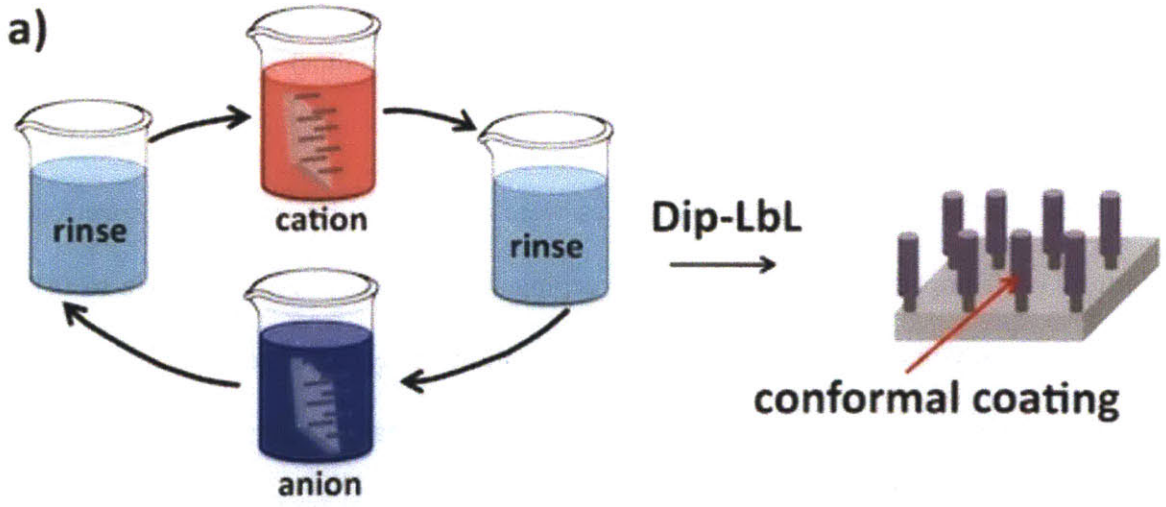

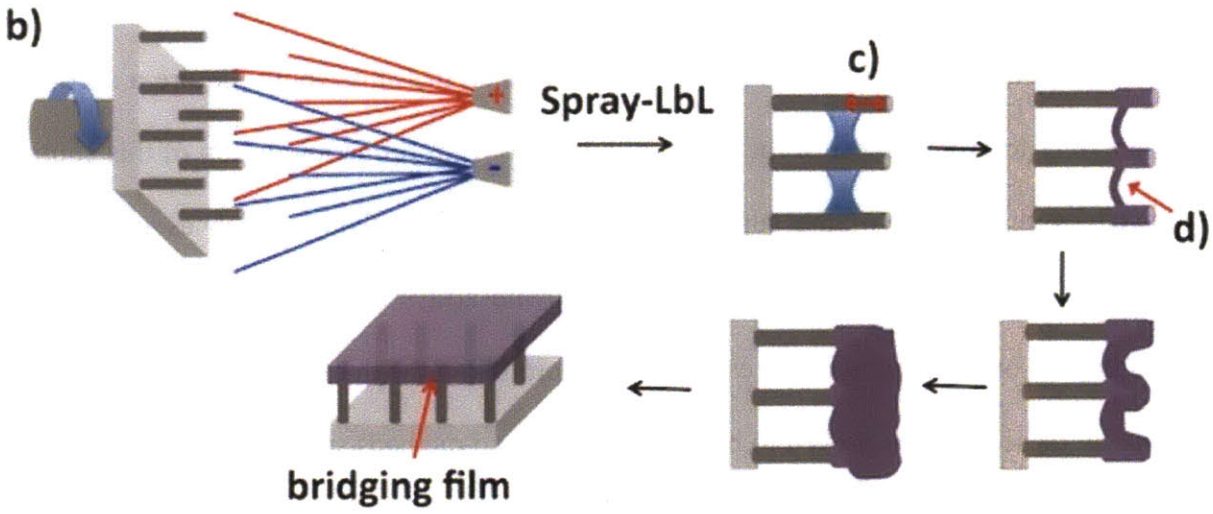

Figure 2.1 **a**) Schematic illustrating the Dip-LbL process and the resulting films that conformally coat high aspect-ratio rods. **b**) Schematic illustrating the Spray-LbL set-up and the proposed formation of a bridging film on a rod array. **c**) The sprayed solution forms capillary bridges between the wires. **d**) Polyelectrolyte complexation results in film formation on the meniscus of the capillary bridges.

2.3.1 Differences in film arrangement with Dip and Spray-LbL on microwire arrays

Layer-by-layer assembly has been touted for its ability to conformally coat complex substrates, so our initial hypothesis was that coating high aspect ratio microwire arrays with LbL films would result in conformal coating along the entire length of the wires. For example, LbL has been shown to generate conformal coatings in nanofluidic devices with aspect ratios of 20–75 (resulting from lateral dimensions of 200–500 nm and depths of 10–15 μm).[16] The microwire substrates examined in this study have aspect ratios of 14–55 for the 1.8 μm diameter wires with heights ranging from 25–100 μm.

Since we were interested in generating structures in which the wires were only partially embedded in an LbL membrane, we anticipated that this would require a sacrificial base polymer to protect most of the wires, allowing for film formation on top of this support, followed by dissolution of the support. Sacrificial support polymers such as polystyrene, estane, and mounting wax were applied to microwire arrays by dropcasting or spincasting from solution, or melting on in the case of wax. Controlling the thickness of the base polymer coating by these methods proved to be very difficult, and methods such as plasma etching and HF etching were examined in order to modify the coating height.

However, building films by Spray-LbL on these partially filled-in wire arrays yielded a surprising result: the LbL film formed a bridging film spanning the tops of the wires floating above (not resting on) the base polymer (Figure 2.2).

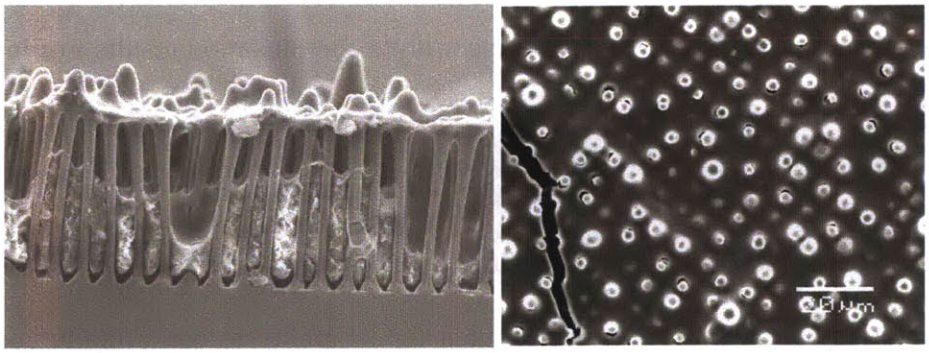

Figure 2.2. **a**) SEM cross-sectional view of a Si microwire array with a polystyrene base polymer and 100 BL PDAC/sPPO LbL bridging film. **b**) Top view of the same array showing a continuous bridging film.

To investigate the causes and controlling factors for this bridging behavior and to probe how the choice of LbL platform controls the location of film formation on high aspect ratio wires, we coated silicon wire arrays with PDAC/sPPO films via Dip-LbL with an incubation time on the order of minutes and contrasted them with wires coated by Spray-LbL

with polymer spray times on the order of seconds. Key differences include the fact that in the dip experiments, the microwire substrate is fully immersed in the dilute polymer aqueous solutions and rinse baths, and polyelectrolyte is allowed to adsorb during the several minute soak period. In the case of Spray-LbL, the sample is exposed to short second-long bursts of aerosolized water droplets that impact the surface of the array, which is oriented such that the top surfaces of the microwires face the direction of flow.

First we consider the case of adsorption of the LbL films using the more traditional dip adsorption process on oxygen plasma treated silicon microwire surfaces, which have a thin layer of oxide on the surface that presents a negative charge. As shown in Figure 2.3a, dipped films of PDAC/sPPO (assembled at pH 2 with 0.2 M NaCl) conformally coat the wires down to a depth of 75 μm. The coatings generated are 500 nm for 25 bilayers; this number corresponds to a linear film growth rate of 20 nm per bilayer pair. This growth rate is consistent with that observed for dipped PDAC/sPPO films on a planar silicon substrate. The conformal coating was consistent with our hypothesis, but the limited penetration (75 μm of the total 100 μm of the wire) was unexpected. The limited penetration of LbL films in this process is likely due to thin pockets of air retained near the base of the immersed arrays, as all surfaces exposed over this extended time period to the solution should have an adsorbed layer of polyelectrolyte. The complete wetting of the array structure appears to have not been achieved in these systems; this phenomenon may be due in part to limitations in the depth of penetration of the cleaning solutions and plasma treatments, which may result in less hydrophilic or even hydrophobic surfaces of silicon near the base of the array. Alternatively, one might posit that the contact angle of water on these surfaces is insufficiently low for capillary forces needed to fully wet the wires. This should be dependent on the interfacial

tension at the air-water interface within the microarray, which in turn would vary with the spacing or packing density of the wires. Wire array wetting and surface chemistry will be discussed in further detail in section 2.3.5.

Figure 2.3 a) A dipped 25 BL PDAC/sPPO (0.2 M NaCl) film conformally coated 100 µm tall silicon microwires to a depth of 75 µm. The clustering of the wires due to capillary forces while drying is reversible, as shown in the top down optical microscope images of the same sample in a **b)** wet and **c)** dry state. **d)** A sprayed 50 BL PDAC/sPPO film only coated the top 10 µm of the silicon microwires.

By contrast, the sprayed films conformally coat only the top 10 µm of the wires (Figure 2.3d). Unlike the fully immersed samples, the Spray-LbL process involves the propulsion of droplets onto a microwire array, which is predominantly surrounded by air. Impact of droplets leads to pinning of the drops across the tops of the microwire arrays and formation of capillary bridges spanning the spaces between the wires. The array is oriented sideways (as shown in Figure 2.1), thus gravity does not force the water deeper into the array. The polyelectrolytes are very dilute aqueous solutions, so they have high surface tension characteristic of water (Table 2.1). High surface tension solutions further favor formation of

capillary bridges. As the next polyelectrolyte solution is sprayed, polyelectrolyte complexation happens on the meniscus of the capillary bridge, setting the limit of film penetration into the array. For this reason, the film forms on the exposed portions of the wires and along the water meniscus that bridges the void space between the wires (Figure 2.1), thus forming a bridging film across the top of the entire array. As the array is then alternately spray-rinsed and exposed to the oppositely charged polyion in the next steps, the LbL complex forms and builds upwards from the location of the original meniscus.

Solution	Concentration (mM)	Surface Tension (mN/m)
Water		71.99 ± 0.05
PDAC	10	71.02 ± 0.01
LPEI	20	71.25 ± 0.01
sPPO	10	68.71 ± 0.03
PAA	20	68.29 ± 0.01

Table 2.1. Surface tension of polyelectrolyte spray solutions.

To take advantage of this interesting phenomenon, we would need to control the penetration depth of the initial capillary bridge (and thus of the film) into the array. The main forces involved are capillary forces and convective forces due to the kinetic energy of the sprayed water droplets. If capillary wicking were the controlling factor, changes in surface chemistry of the wires and in spacing of the array would be expected to have dramatic effects on the penetration depth. If convective forces were controlling, parameters related to the amount of solution sprayed and the spray time would be expected to have a greater effect on

the penetration depth. The effects of changing these parameters are explored in the following sections.

2.3.2 Effect of spray time and spray pressure on film penetration depth

To further understand the mechanism that controls the film penetration depth, the effect of spray time and spray pressure was examined. A previous optimization study of Spray-LbL parameters[17] showed that increasing polyion spray time led to increases in film thickness and roughness. For films sprayed on microwire arrays, increased spray time also increased film penetration depth (Figure 2.4a-b). Once a capillary bridge forms between the wires, the impact of subsequent drops of solution transfers the kinetic energy of the drops to the capillary bridge and pushes it further into the array.

Likewise, increased air pressure leads to an increase of impact velocity of the drops on planar substrates, and a subsequent increase of film thickness and roughness.[17] [Note: the air pressure controls the impact velocity, but not the flow rate: the number of turns of the air nozzle controls the flow rate, which was not varied in this work. A flow rate of 0.25–0.3 mL/s was used]. With microwire array substrates, increasing the spray pressure above 20 psi led to an increase in film penetration depth variability, but no statistically meaningful change in mean film depth (Figure 2.4c). Spraying at 15 psi however led to a decrease of film depth. At 15 psi, there is a longer delay between when the air spray starts and when the liquid is pulled up and starts spraying, so this decrease in film depth is likely explained by a decreased spray time. Polymer spray time is one of the main controlling factors of the film penetration depth of films sprayed on microwire arrays.

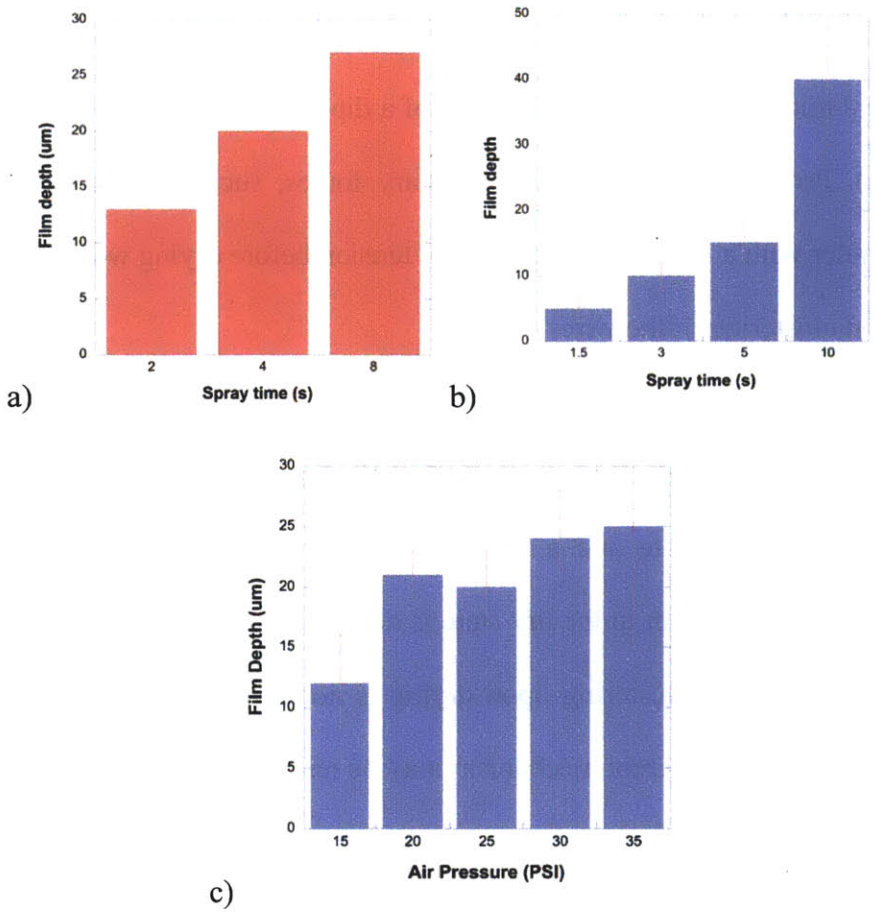

Figure 2.4 Increasing the polymer spray increases the film penetration depth for **a)** LPEI/PAA and **b)** PDAC/sPPO LbL films. **c)** Spray pressure versus film penetration depth for LPEI/PAA films.

2.3.3 Wire clustering and critical thickness to observe film bridging in dry state

The silicon wire arrays studied here are vertically oriented and regularly spaced, but after coating with LbL films, wire bending and clustering was often observed in the dry state. Two forces are likely responsible for this behavior: capillary forces and film deswelling. In the case of Dip-LbL, the wire arrays are fully immersed in solution, and as the array dries, capillary forces bend the wires and leave them clustered together. The cohesive forces in the water and the adhesive forces between the water and the wire surfaces are greater than the

force required to bend the wires, leading to wire clustering. This process is reversible as shown in optical microscope pictures of the top of a dip-coated array in the dry and wet states (Figure 2.3b-c). Processes that minimize capillary forces, such as supercritical drying, or replacing the water with a liquid of lower surface tension before drying would likely eliminate this bending and clustering of the wires.

However, in the Spray-LbL case, clustering and bending is only observed when lower numbers of bilayers are sprayed, above a certain thickness, the wires remain vertical and evenly spaced in the dry state and a bridging film is observed spanning between them. Observation of the bridged film in the dry state is dependent on the thickness and mechanical properties of the film. The clustering upon drying is not reversible as seen in the Dip-LbL case. This indicates that a different mechanism may be responsible for the clustering observed in the sprayed wire arrays. Free-standing PDAC/sPPO films swell significantly in water (16%), hence upon drying in air, the films contract as they lose water. Thus a competition occurred between the shrinking-induced strain and the elastic modulus and dimensions of the film. For very thin films, the strain predominates, and the bridging films will tear during handling and drying; thus they were not observed in the dry state, and wire clustering and bending is observed. However, above a critical thickness of ~ 2 μm the films were no longer susceptible to rupture upon de-swelling, allowing the resulting bridged films to be observed in the dry state. The rate of water removal can be controlled to address or impact film rupture to some extent; for example, an acceleration of the drying process by drying films under a hot optical microscope lamp led to rupture of films up to 3.5 μm thick (Figure 2.5c-e), and similarly, slow drying in a humidified chamber or supercritical drying is anticipated to lead to the isolation of thinner films in the dry state.

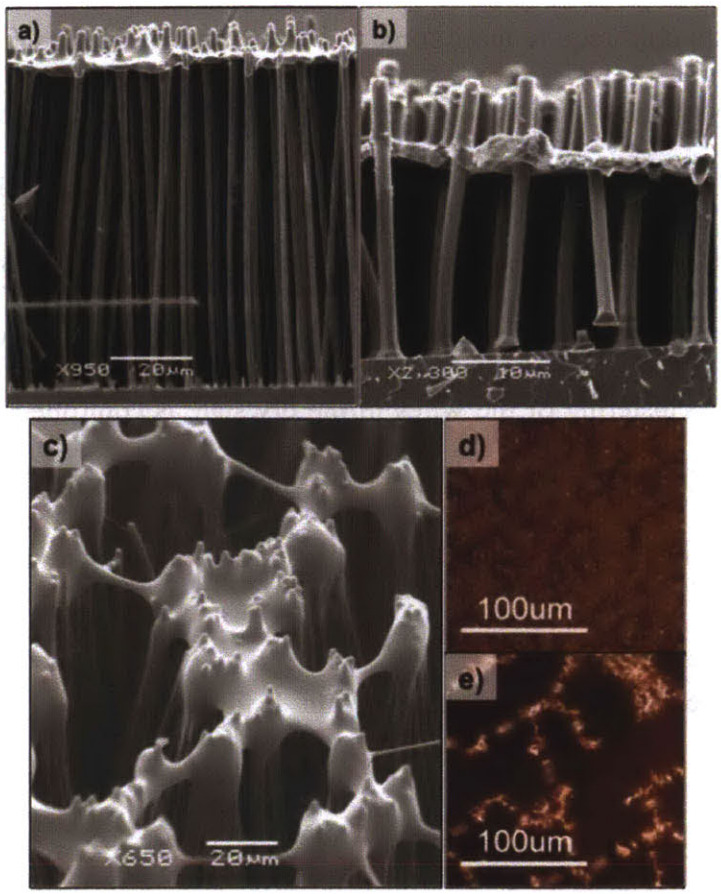

Figure 2.5. Spraying 100 BL of PDAC/sPPO formed bridged films on **a)** 90 μm tall and **b)** 30 μm tall silicon wires. The film penetrates 8 μm into the array in both cases. **c)** A sprayed 75 BL LPEI/PAA film tore due to drying-induced shrinking under the hot light of an optical microscope. **d)** The same film while still wet showed an ordered arrangement of the wires and continuous bridging, **e)** but once it dried, the film was collapsed and ruptured and the wires clustered together. This process was not reversible.

We did not observe an effect of wire height on the critical thickness required to observe film bridging in the dry state (Figure 2.5a-b). Drying hydrogels have been shown to bend high-aspect ratio silicon wires,[18] and we hypothesized that varying the aspect ratio of the wires would change the force required to bend the wires and thus effect the critical thickness

value. Shorter wires would require more force to bend them, so capillary forces during drying may not be strong enough to bend and cluster the wires, this would allow bridging films to be observed at lower thickness values in the dry state. However this hypothesis was proven false for this system at the aspect ratios studied, as the critical bridging thickness was the same for both 90 μm and 30 μm tall wires (with aspect ratios 50 and 16.6 respectively). It is possible that the bending and clustering of the wires in the dry state is controlled by capillary forces during drying (reversible process) in the case of the dipped wires, but is largely controlled by film deswelling and rupture (irreversible process) in the case of the sprayed wires.

2.3.4 Impact of microwire array spacing on film bridging

We examined the effect of wire array diameter and spacing, spraying films on wire arrays with three different geometries (Table 2.2). Previous studies of Spray-LbL on porous membranes found that pores smaller than the 5 μm droplet size of the spray can be bridged, and that slightly larger pores (~ 10 um) can be bridged due to favorable interfacial interactions.[10b] Pores greater than 200 μm were also shown to be bridged via polyelectrolyte complex accumulation in droplets created by a Rayleigh–Taylor instability.[19] The results of the current study are consistent with the findings of these pore-bridging studies. The two wire array geometries with empty spans smaller than 10 μm exhibited bridging and film penetration depth was the same in these systems, keeping other parameters constant. The penetration depth being unaffected by wire spacing below a certain size is consistent with the proposed mechanism of convective forces setting the penetration depth. If the depth were set by capillary wicking into the array, changing the spacing would be expected to change the capillary forces and thus the depth of penetration into the array.

In the case of wire arrays with empty spans larger than 10 μm, bridging was not observed, and the wires were conformally coated along their entire length (Figure 2.7a). However, as thicker films were sprayed on the wires, increasing their effective diameter and shrinking the empty space between the wires closer to 10 μm, bridging began to be observed (Figure 2.7b-d). Top-down SEM images show incomplete bridging coverage and empty spaces between the wires of 8-9 μm. The bridging film penetration depth in this case was again the same as for the sets of more closely packed wires.

Radius μm	Pitch μm	Packing Geometry	Span μm
0.35	2.5	square	1.8 - 2.8
0.9	7	square	5.2 - 8.1
3.75	20	hexagonal	12.5 - 27.5

Table 2.2. Wire array sizes and spacing. The empty space between the surface of one wire and its nearest neighbors is listed in the "Span" column.

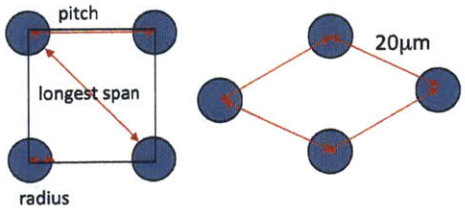

Figure 2.6 Illustration of square and hexagonal wire packing geometries.

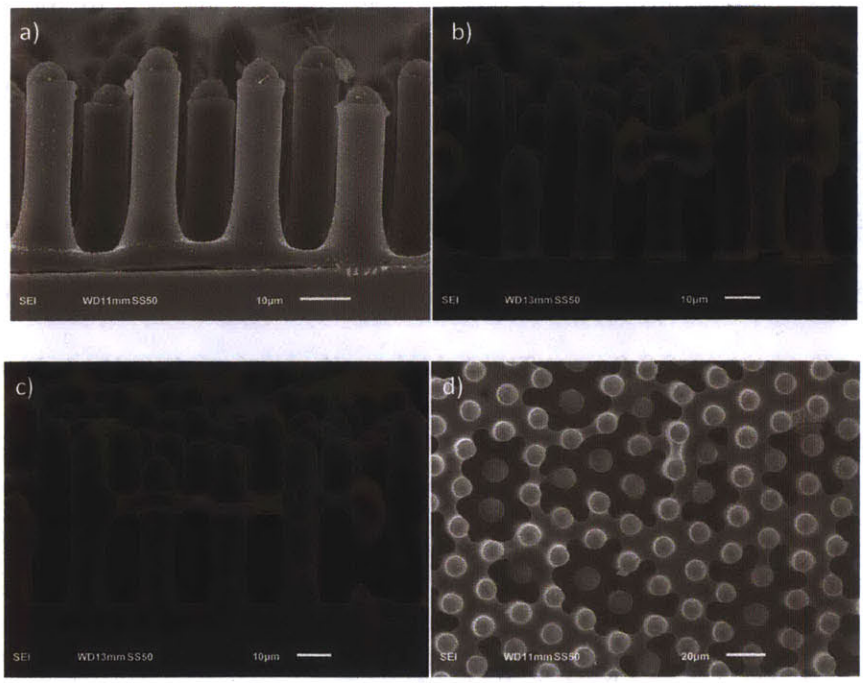

Figure 2.7 a) A sprayed 50BL PDAC/sPPO film on 7.5 μm diameter wires conformally coated the entire length of the wires. **b-c)** A sprayed 100 BL LPEI/PAA film on the same size wire array also conformally coated the length of the wires, but started to bridge in some areas once the space between the wires was smaller. **d)** A top-down view of the same sample shows incomplete bridging coverage.

2.3.5 Effect of silicon surface chemistry on wetting properties and film penetration depth

The capillary forces involved in film bridging can be modulated by changing the surface energy of the wires. We probed the effect of surface wetting properties by studying three different silicon surface chemistries: H-terminated, OH-terminated, and $(CH_2)_2(CF_2)_5CF_3$ terminated. The water contact angles of planar silicon with these surface chemistries were 75°, 24°, and 102° respectively (Figure 2.8). For the two hydrophilic surfaces (water contact angles less than 90°), an initial contact angle for the wire array could be measured, but within seconds the water drop spread out and disappeared from view as

capillary forces drew the water into the void space between the wires. This behavior is consistent with the Wenzel wetting model: roughness increases the surface area, which also geometrically modifies the wetting properties. In contrast, the hydrophobic wires (water contact greater than 90°) displayed a water contact angle of 150°. The wire array is more hydrophobic than the planar surface, as explained by the Cassie wetting model for a liquid on a composite surface in which one component is air.[20] Air remains trapped below the water drop, increasing the hydrophobicity of the array because the drop sits partially on air (which has a contact angle of 180°).

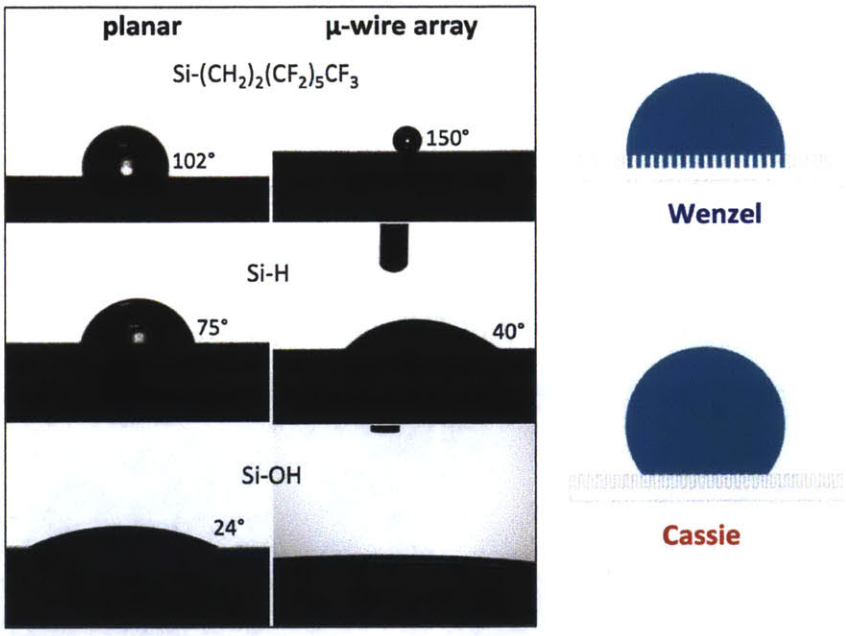

Figure 2.8 Water contact angles on planar Si and microwires. Cartoons illustrating the expected behavior for the Wenzel and Cassie wetting models. Wires with hydrophilic Si surfaces follow the Wenzel model, while wires with hydrophobic surfaces follow the Cassie model.

As expected, the surface chemistry of the silicon wires had a dramatic effect on the film arrangement. Films penetrated twice as far into the hydroxyl-terminated (Si-OH)

hydrophilic arrays than into the much more hydrophobic perfluorinated (Si-$(CH_2)_2(CF_2)_5CF_3$) arrays (Figure 2.9). Interestingly, there was no discernable difference between the Si-H and the Si-OH surface chemistries, which were coated to equal depths; though it is worth noting that both contact angles are below 90° for these two cases, making them both hydrophilic. This indicates that there may be a switch in whether silicon surface wettability is the controlling factor in determining penetration depth. For contact angles above 90°, capillary forces may dominate, but for surfaces with contact angles below 90° other factors such as convective forces control the penetration depth of the film. This general phenomenon was consistent when the polyelectrolyte ion pair was changed from PDAC/sPPO to the weak acid/base pair, LPEI/PAA. This switch in behavior between surface chemistry and other factors controlling penetration depth of the film was also observed with Dip-LbL. Hydrophilic wires were conformally coated to greater than 50 μm as discussed previously, but bridging films formed atop hydrophobic (Si-CH_3) wires (Figure B.2).

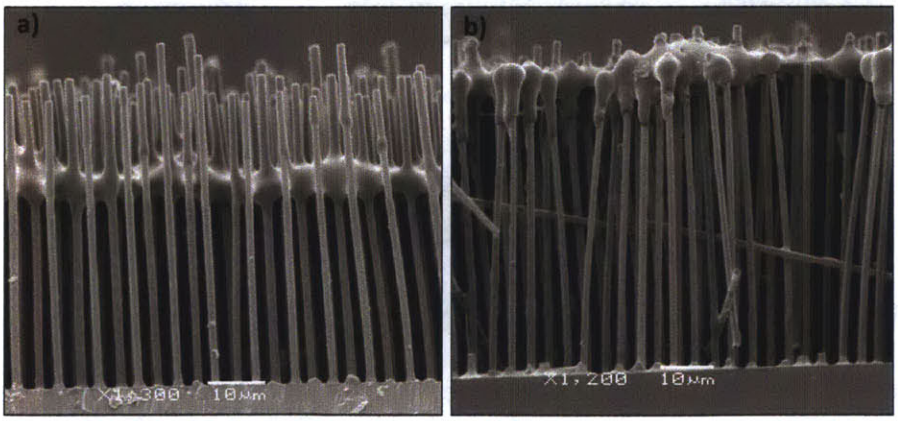

Figure 2.9 Sprayed 75 BL films of LPEI/PAA on a) hydrophilic Si-OH terminated wires and b) hydrophobic Si-$(CH_2)_2(CF_2)_5CF_3$ terminated wires. The film penetrated 10 ± 3 μm into the hydrophilic array, but only half as far, 5 ± 2 μm, into the hydrophobic array.

2.3.6 Use of Spray-LbL to fabricate microwire composite structures

To demonstrate the utility of spray-LbL to embed and support microwire arrays, thick (>8 μm) bridging films were assembled on the wires, followed by mechanically detaching the wires from the substrate to yield free-standing LbL membranes (Figure 2.10). To mechanically detach the wires, the substrate was glued to a glass slide to hold it firmly in place, then a razor blade was applied at an angle to the edge of the array and scrapped across the array with constant pressure, thus breaking the attachment between the base of the wires and the substrate without damaging the LbL film. The LbL films acted as structural supports for the wires and maintained the ordered arrangement of the original array.

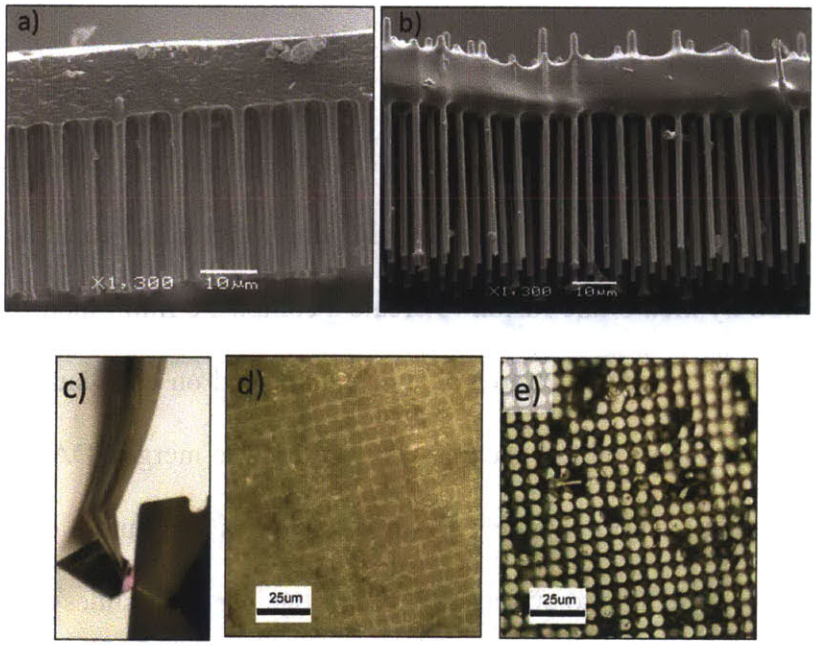

Figure 2.10. A Free-standing membranes of **a)** 250 BL PDAC/sPPO and **b)** 250 BL LPEI/PAA can support the embedded wire arrays and retained the ordered arrangement of the wires. **c)** Mechanically detaching the wires from the substrate with a razor blade. Optical microscope images of the **d)** top and **e)** bottom of a wire array in a free-standing LbL film.

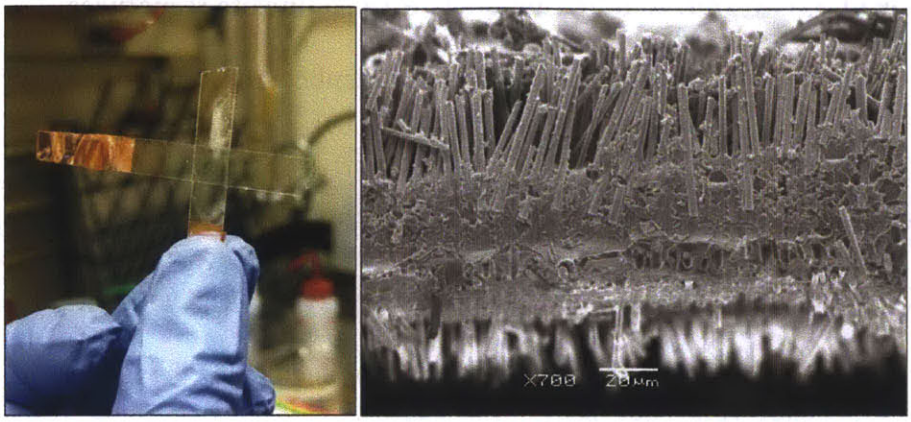

Figure 2.11. a) Merged 300BL PDAC/sPPO films holding together glass slides. When attempting to separate the slides, the glass broke before the film could be broken. **b)** Two free-standing membrane wire assemblies of 250 BL PDAC/sPPO were merged together to create a continuous film supporting a double stack of Si wires.

A further advantage of using LbL films as functional membranes to support electrode arrays is that LbL films can be merged together, allowing for modular construction of separate membranes followed by membrane fusion to create a composite film. Such films can act as a connecting medium for Si wire electrodes that are embedded on each side of the polymeric layer. Herein such multilayer-transfer techniques were used to merge PDAC/sPPO LbL films by pressing together films with oppositely charged top layers in a humid environment. Films merged in this manner were able to effectively "glue" together glass slides (Figure 2.11a). 300 BL PDAC/sPPO films on glass were subjected to 90% relative humidity (RH) for 30 min, then held in contact with a binder clip for 24 hr at 90% RH. The binder clip was removed and the films were allowed to dry at ambient humidity for 24 hr. When attempting to manually separate the slides after this merging process, the glass broke before the films could be separated. This technique was also extended to assemble multicomponent dimensional structures, by merging free-standing ionically conducting membrane-microwire assemblies

into a single functional film (Figure 2.11b). The humidified free-standing membranes were placed in contact between glass microscope slides with a 25 g weight on top for 24 hr at 90% RH. Cross-sectional SEM micrographs showed no visible gap or distinction between the two membranes, indicating that continuous merging of the membranes had occurred.

To determine whether the interface between the merged films presented a barrier to ionic conductivity, PDAC/sPPO films were merged at various conditions, and analyzed with impedance spectroscopy (Table 2.3). Because of the very thin (< 20 μm) dimensions of these films, the overall conductance was high, hence the conductivity was measured at low humidity conditions so as to stay within the detection range of the equipment, but it should be noted that the ionic conductivity increases greatly with humidity, and at 98% RH the conductivity of a single PDAC/sPPO film is 0.012 Scm^{-1}. Changing assembly ionic strength conditions and/or using a more highly sulfonated batch of sPPO can yield higher values.[12b]

Films were merged by subjecting films with oppositely charged top layers (ending on either PDAC or sPPO) to either humidity or a drop of solution, and then placing the films in contact under pressure (see section 2.2.6 for experimental details). Merging films with humidity alone was found to be the least consistent method in terms of time needed for merging and resistivity of the interface. Solution-based merging methods were more effective. The presence of salt was also found to be critical to the merging process; films that were soaked in deionized water to remove excess salt would not merge unless excess salt was reintroduced. When the excess charge at the surface of a polyelectrolyte multilayer film is mostly compensated by salt ions, those charges are available to interact with an oppositely charged polymer surface because the salt is easily displaced. However, when the excess surface charge is intrinsically compensated by the neighboring oppositely charged polymer

layer in the film, which cannot be easily displaced, the film will not form electrostatic cross-links with the charged surface of an adjacent film.[21]

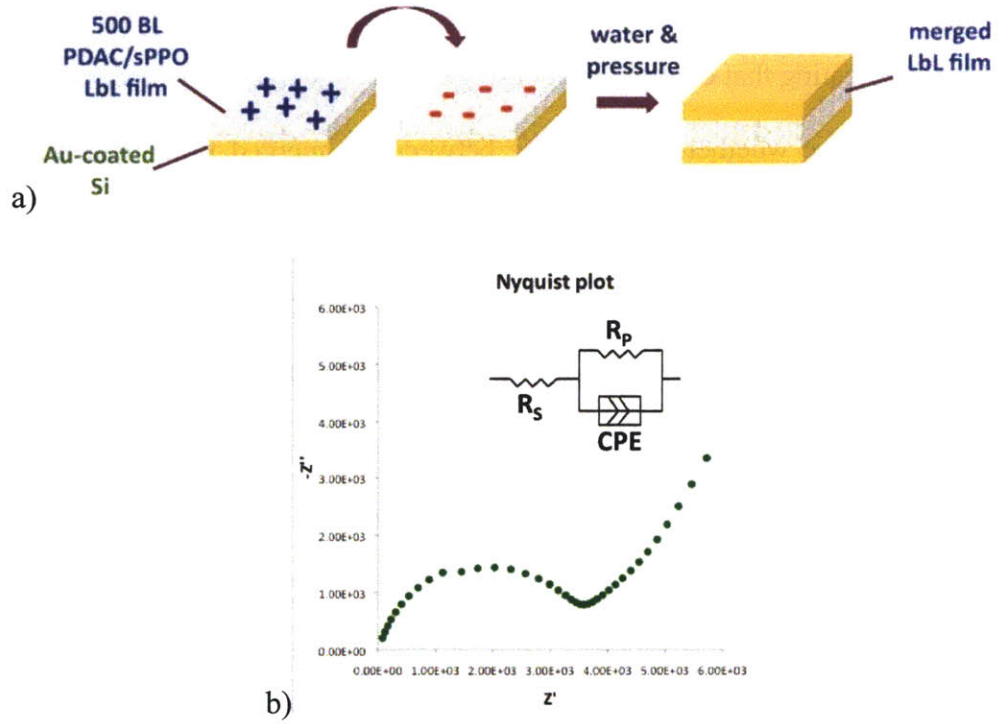

Figure 2.12. **a**) Schematic of experiment to measure resistance across the interface of merged films. **b**) Representative Nyquist plot and the equivalent circuit used to model the data.

Sample	σ 35% RH [Scm^{-1}]	σ 60% RH [Scm^{-1}]
Single Film	2×10^{-6}	5×10^{-5}
Merged w/ sPPO solution	5×10^{-5}	1×10^{-4}
Merged w/ PDAC solution	3×10^{-6}	6×10^{-5}
Merged w/ 0.5 M NaCl soln	6×10^{-6}	7×10^{-5}
Merged w/ humidity	2×10^{-6}	4×10^{-5}
Clipped together dry	N/A	3×10^{-10}

Table 2.3 Ionic conductivity of 500 bilayer PDAC/sPPO films on glass and of merged 500 BL PDAC/sPPO films on Au-coated Si at various humidity levels.

Films that had been merged with sPPO solution were twice as conductive as single films, indicating that additional sPPO had been incorporated into the bulk of the film, increasing the number of sites for ionic charge transport. The other merging conditions resulted in films that had ionic conductivities of the same order of magnitude as a single film, hence the interface did not create a significant resistive barrier to ion transport. Pressing together dry films, with no attempt to merge them, resulted in a significant resistive barrier, further demonstrating that the merging conditions change the interface of the films. [The conductivity of merged films was measured after the pressure (binder clip or 25 g weight) was removed, but the unmerged films that were pressed together while dry were measured while held in contact with a binder clip.] Separate films could therefore be assembled and merged while retaining their functionality. Transfer printing has not previously been used for 3-dimensional assembly and functionality in this manner.

2.4 Conclusion

Spray-LbL assembly has been used to embed and transfer vertically aligned Si microwire arrays into free-standing ion-conducting functional membranes. We have further assembled multicomponent dimensional structures, by merging free-standing membrane-microwire assemblies into a single functional film, demonstrating the extension of multilayer assembly and transfer to 3-D microfabrication. This technique appears to be general and could be extended to other types of functional LbL films, such as electrically or mixed conductive films, as well as films with tunable permeability to molecules, enabling the assembly of complex devices that could be adapted to mediate transport between active components. The ability to control the thickness of the film, to fine tune its composition along

the *z*-direction, and to limit film formation to specific regions of the wire array on the micron-scale are attractive features of this method that distinguish it from the use of bulk polymers. Ultimately, this set of approaches could offer options relative to traditional materials for microfabrication of Si devices such as solar-driven water splitting systems, capacitors, or electrochemically active electrodes.

2.5 References

1. (a) Kelzenberg, M. D.; Turner-Evans, D. B.; Putnam, M. C.; Boettcher, S. W.; Briggs, R. M.; Baek, J. Y.; Lewis, N. S.; Atwater, H. A., High-performance Si microwire photovoltaics. *Energy & Environmental Science* **2011,** *4* (3), 866-871; (b) Spurgeon, J. M.; Boettcher, S. W.; Kelzenberg, M. D.; Brunschwig, B. S.; Atwater, H. A.; Lewis, N. S., Flexible, Polymer-Supported, Si Wire Array Photoelectrodes. *Advanced Materials* **2010,** *22* (30), 3277-+; (c) Chu, S.; Li, D.; Chang, P.-C.; Lu, J. G., Flexible Dye-Sensitized Solar Cell Based on Vertical ZnO Nanowire Arrays. *Nanoscale Research Letters* **2011,** *6*; (d) Garnett, E.; Yang, P., Light Trapping in Silicon Nanowire Solar Cells. *Nano Letters* **2010,** *10* (3), 1082-1087.
2. (a) Lewis, N. S.; Nocera, D. G., Powering the planet: Chemical challenges in solar energy utilization. *Proc. Natl. Acad. Sci. U.S.A.* **2006,** *103*, 15729-15735; (b) Spurgeon, J. M.; Walter, M. G.; Zhou, J.; Kohl, P. A.; Lewis, N. S., Electrical conductivity, ionic conductivity, optical absorption, and gas separation properties of ionically conductive polymer membranes embedded with Si microwire arrays. *Energy & Environmental Science* **2011,** *4* (5), 1772-1780; (c) McFarlane, S. L.; Day, B. A.; McEleney, K.; Freund, M. S.; Lewis, N. S., Designing electronic/ionic conducting membranes for artificial photosynthesis. *Energy & Environmental Science* **2011,** *4*, 1700-1703.
3. (a) Abramson, A. R.; Kim, W. C.; Huxtable, S. T.; Yan, H. Q.; Wu, Y. Y.; Majumdar, A.; Tien, C. L.; Yang, P. D., Fabrication and characterization of a nanowire/polymer-based nanocomposite for a prototype thermoelectric device. *Journal of Microelectromechanical Systems* **2004,** *13* (3), 505-513; (b) Boukai, A. I.; Bunimovich, Y.; Tahir-Kheli, J.; Yu, J.-K.; Goddard Iii, W. A.; Heath, J. R., Silicon nanowires as efficient thermoelectric materials. *Nature* **2008,** *451* (7175), 168-171; (c) Hochbaum, A. I.; Chen, R.; Delgado, R. D.; Liang, W.; Garnett, E. C.; Najarian, M.; Majumdar, A.; Yang, P., Enhanced thermoelectric performance of rough silicon nanowires. *Nature* **2008,** *451* (7175), 163-167.
4. (a) Goldberger, J.; Hochbaum, A. I.; Fan, R.; Yang, P., Silicon Vertically Integrated Nanowire Field Effect Transistors. *Nano Letters* **2006,** *6* (5), 973-977; (b) Lugstein, A.; Steinmair, M.; Henkel, C.; Bertagnolli, E., Scalable Approach for Vertical Device Integration of Epitaxial Nanowires. *Nano Letters* **2009,** *9* (5), 1830-1834.
5. Weisse, J. M.; Kim, D. R.; Lee, C. H.; Zheng, X., Vertical Transfer of Uniform Silicon Nanowire Arrays via Crack Formation. *Nano Letters* **2011,** *11* (3), 1300-1305.

6. Plass, K. E.; Filler, M. A.; Spurgeon, J. M.; Kayes, B. M.; Maldonado, S.; Brunschwig, B. S.; Atwater, H. A.; Lewis, N. S., Flexible Polymer-Embedded Si Wire Arrays. *Advanced Materials* **2009,** *21*, 325-328.
7. Kim, D.-H.; Ahn, J.-H.; Choi, W. M.; Kim, H.-S.; Kim, T.-H.; Song, J.; Huang, Y. Y.; Liu, Z.; Lu, C.; Rogers, J. A., Stretchable and Foldable Silicon Integrated Circuits. *Science* **2008,** *320*, 507-511.
8. Kayes, B. M.; Atwater, H. A.; Lewis, N. S., Comparison of the device physics principles of planar and radial p-n junction nanorod solar cells. *Journal of Applied Physics* **2005,** *97*, 114302.
9. (a) Decher, G., Fuzzy Nanoassemblies: Toward Layered Polymeric Multicomposites. *Science* **1997,** *277*, 1232; (b) Lutkenhaus, J. L.; Hammond, P. T., Electrochemically enabled polyelectrolyte multilayer devices: from fuel cells to sensors. *Soft Matter* **2007,** *3* (7), 804-816.
10. (a) Krogman, K. C.; Zacharia, N. S.; Schroeder, S.; Hammond, P. T., Automated Process for Improved Uniformity and Versatility of Layer-by-Layer Deposition. *Langmuir* **2007,** *23* (6), 3137-3141; (b) Krogman, K. C.; Lowery, J. L.; Zacharia, N. S.; Rutledge, G. C.; Hammond, P. T., Spraying asymmetry into functional membranes layer-by-layer. *Nature Materials* **2009,** *8* (6), 512-518; (c) Izquierdo, A.; Ono, S. S.; Voegel, J. C.; Schaaf, P.; Decher, G., Dipping versus Spraying: Exploring the Deposition Conditions for Speeding Up Layer-by-Layer Assembly. *Langmuir* **2005,** *21* (16), 7558-7567.
11. DeLongchamp, D. M.; Hammond, P. T., Fast Ion Conduction in Layer-By-Layer Polymer Films. *Chemistry of Materials* **2003,** *15* (5), 1165-1173.
12. (a) Argun, A. A.; Ashcraft, J. N.; Hammond, P. T., Highly Conductive, Methanol Resistant Polyelectrolyte Multilayers. *Advanced Materials* **2008,** *20*, 1539-1543; (b) Ashcraft, J. N.; Argun, A. A.; Hammond, P. T., Structure-property studies of highly conductive layer-by-layer assembled membranes for fuel cell PEM applications. *Journal of Materials Chemistry* **2010,** *20*, 6250-6257.
13. Jiang, X.; Zheng, H.; Gourdin, S.; Hammond, P. T., Polymer-on-Polymer Stamping: Universal Approaches to Chemically Patterned Surfaces. *Langmuir* **2002,** *18* (7), 2607-2615.
14. Park, J.; Hammond, P. T., Multilayer Transfer Printing for Polyelectrolyte Multilayer Patterning: Direct Transfer of Layer-by-Layer Assembled Micropatterned Thin Films. *Advanced Materials* **2004,** *16*, 520-525.
15. Park, J.; Kim, Y. S.; Hammond, P. T., Chemically Nanopatterned Surfaces Using Polyelectrolytes and Ultraviolet-Cured Hard Molds. *Nano Letters* **2005,** *5* (7), 1347-1350.
16. DeRocher, J. P.; Mao, P.; Han, J.; Rubner, M. F.; Cohen, R. E., Layer-by-Layer Assembly of Polyelectrolytes in Nanofluidic Devices. *Macromolecules* **2010,** *43* (5), 2430-2437.
17. Gifford, J. H. Optimization of the Automated Spray Layer-by-layer Technique for Thin Film Deposition. Massachusetts Institute of Technology, 2010.
18. Sidorenko, A.; Krupenkin, T.; Taylor, A.; Fratzl, P.; Aizenberg, J., Reversible Switching of Hydrogel-Actuated Nanostructures into Complex Micropatterns. *Science* **2007,** *315*, 487-490.
19. Ladewski, R. L. Investigation of Layer-by-layer Assembly and M13 Bacteriophage Nanowires for Dye-Sensitized Solar Cells. Massachusetts Institute of Technology, 2012.
20. Cassie, A. B. D.; Baxter, S., Wettability of porous surfaces. *Transactions of the Faraday Society* **1944,** *40*, 546-551.

21. Schlenoff, J. B.; Dubas, S. T., Mechanism of Polyelectrolyte Multilayer Growth: Charge Overcompensation and Distribution. *Macromolecules* **2001,** *34* (3), 592-598.

Chapter 3.

Highly Transparent Layer-by-Layer Assembled Mixed Conducting Membranes With Tunable Properties

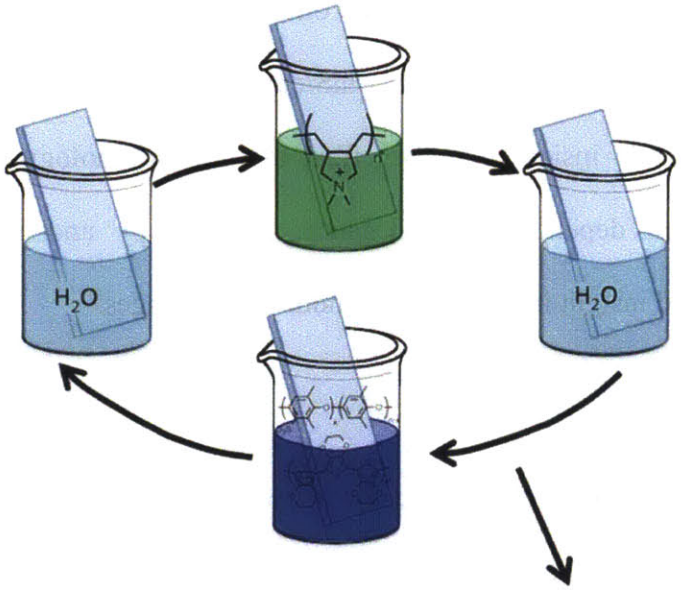

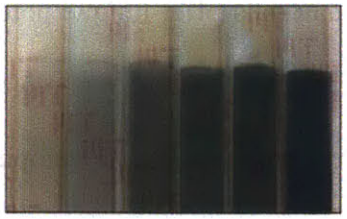

ABSTRACT: Transparent mixed conducting polymer films with conductivity above 0.1 mS/cm are highly desirable for photoelectrochemical cell membrane applications. Mixed conducting polymer composite PEDOT:sPPO was incorporated into LbL films and the composition ratio of the film components was varied to generate a series of films with tunable transparency and electrical and protonic conductivities. The visible light transmission properties are excellent: 1.1 μm thick films with 150 mS/cm electrical conductivity have 80% transmission of light in the visual range. The electronic and ionic conductivities are inversely related, as one can be increased at the expense of the other. The highest ionic conductivity recorded was 4 mS/cm for 4.6 μm thick films with 2 mS/cm electrical conductivity. Electron microscopy was used to provide insight into the effect of film morphology on electrical conductivity, and temperature dependent impededance spectroscopy and ion exchange capacity measurements yielded insight into the ionic conductivity changes.

3.1 Introduction

The design and development of thin films that are highly transparent, and both ionically and electrically conductive (mixed conductors) has garnered tremendous interest because these materials offer unique potential in devices such as battery electrodes, chemical sensors, gas separators, wireless photosynthesis devices, and electrochromic windows.[1] Of particular interest to us is the development of mixed conducting membranes for a solar-powered water-splitting device. Detailed computational modeling of the effect of membrane properties on device efficiencies have identified 0.1 mS/cm as the minimum required conductivity for the mixed conducting membrane in this device design.[2] Ideally the ionic and electrical conductivities would be close to equal, as whichever one is lower will be the determining factor in voltage loss through the membrane.

Poly(3,4-ethylenedioxythiophene) (PEDOT) has been widely applied for electrochromic devices, anti-static coatings, and electrodes due to its high electrical conductivity and high optical transparency.[3] By using the strong sulfonic acid groups of sulfonated poly(dimethyl phenylene oxide) (sPPO) as a doping agent for PEDOT, we have successfully synthesized highly transparent protonically and electrically conductive PEDOT:sPPO (Figure 3.1a-b).[4] However this material cannot be used as a membrane for a device that will be immersed in water, as thin films of it swell and break apart after 12 h in water at ambient conditions. The incorporation of PEDOT:sPPO into films using the LbL adsorption technique is predicted to create water stable, transparent films with both high ionic and electronic conductivities.[5] Furthermore, due to the flexibility of LbL, we can easily tune the membrane transparency, thickness, morphology, and conductivities by different assembly conditions and architectures.

LbL films composed of PDAC/sPPO have been used as proton exchange membranes in direct methanol fuel cells and this system can reach ionic conductivities of 70 mS/cm when fully humidified.[5] We hypothesized that to combining this proton conducting system with the mixed conducting PEDOT:sPPO would result in films with proton and electrical conductivities in the desired range for the solar water-splitting application.

In this study, two LbL assembly architectures were investigated to tune the polymer transparency and conductivities; a bilayer architecture of PEDOT:sPPO alternating with poly(dimethyl diallyl ammonium chloride) (PDAC) (Figure 3.1c), and a tetralayer architecture that replaced every other PEDOT:sPPO layer in the bilayer films with sPPO. The use of added salts in the film assembly baths in order to further increase the composition ratio of the highly protonically conducting sPPO was also examined. The LBL film morphologies

were also investigated by TEM and SEM to understand how the morphology effects film conductivities.

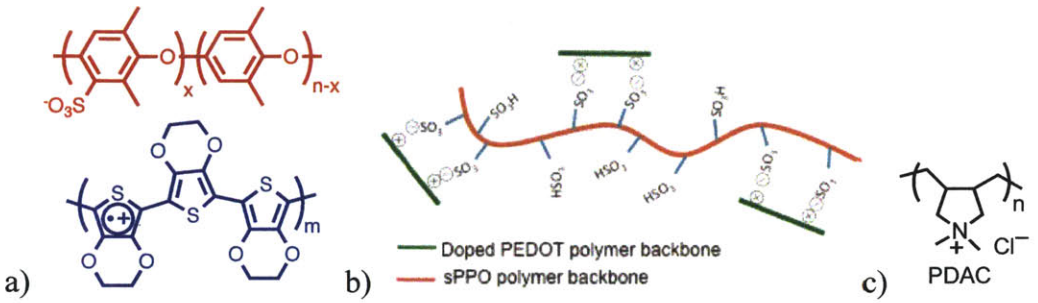

Figure 3.1. **a**) PEDOT was synthesized by oxidative polymerization in an aqueous solution of sPPO, resulting in a polymer blend suspended in solution. The sulfonate groups of sPPO act as dopant for the oxidized PEDOT. **b**) Cartoon of the proposed structure for PEDOT:sPPO. **c**) Structure of the polycation used to generate LbL films in this work.

3.2 Materials and Methods

3.2.1 Polymer Sources and Synthesis: Poly(2,6-dimethyl-1,4-phenylene oxide) (PPO, MW = 23,000), poly(diallyldimethylammonium chloride) (PDAC, MW = 240,000), 3,4-ethylenedioxythiophene (EDOT), and all other solvents and reagents were obtained from Sigma-Aldrich.

Synthesis of sPPO: An oven-dried 2 L 3-neck round-bottom flask was fitted with an overhead mechanical stirrer, a condenser, and an inert gas inlet. The apparatus was cooled under nitrogen, and charged with PPO (5 g, 41.6 mmol). The apparatus was evacuated and backfilled with nitrogen, this process was repeated three times. Chloroform (50 mL) and 1,2-dichloroethane (400 mL) were added. (Anhydrous solvents were obtained from Sigma Aldrich in sure-seal bottles). The reaction vessel was heated at 45°C overnight with vigorous stirring to ensure that the PPO was fully dissolved. The temperature was increased to 80°C

and a mixture of trimethylsilyl chlorosulfonate (19 mL, 125 mmol) in anhydrous 1,2-dichloroethane (41 mL) was added via syringe pump at a rate of 16 mL/h. The reaction mixture was kept under nitrogen at 80°C with vigorous stirring for 72 hours. After cooling the reaction mixture in an ice bath, the precipitated solids were collected by filtration and dissolved in methanol. The remaining solution was concentrated under reduced pressure, and the residue was extracted with methanol. The methanol solutions were combined, sodium methoxide (2.25 g, 41.6 mmol) was added, and the reaction mixture was allowed to stir overnight to remove the trimethylsilyl protecting groups from the sulfonate groups. The reaction mixture was concentrated under reduced pressure to a volume of ~ 75 mL. The concentrated solution was added drop-wise to a stirred container of acetone (~1 L) cooled in an ice bath. The sodium form of sPPO (sPPO-Na) was collected as white precipitate by vacuum filtration and rinsed with ice-cold acetone. The polymer was then dissolved in deionized water, placed into a 3,500 MW cut-off membrane, and dialyzed against pH 1 water for 2 h, followed by pH 2 water for 2 h to exchange the sodium ions for protons. The polymer solution was then dialyzed against deionized water overnight to remove excess acid. The polymer solution was then filtered and stored as an aqueous stock solution until use.

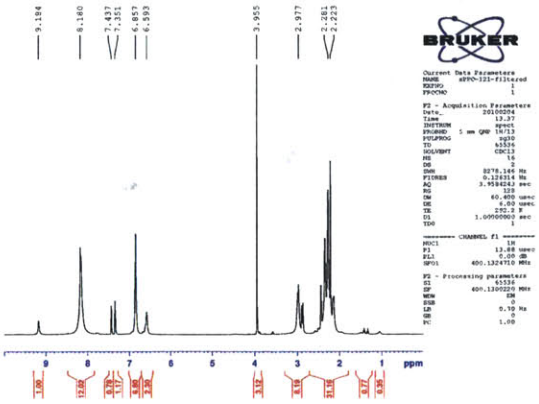

Synthesis of PEDOT:sPPO:[4] An aqueous solution of sPPO (15 mM with respect to repeat unit, 80 ml) was purged of oxygen at 25 °C with nitrogen bubbling for 30 min. EDOT (487 mg, 3.43 mmol) and $Fe_2(SO_4)_3 \bullet 9H_2O$ (7 mg, 0.017 mmol) were then added to the flask to initiate the polymerization. The mixture was then stirred at 25 °C for 7 h, after which $Na_2S_2O_8$ (163 mg, 0.69 mmol) was added. After an additional 14 h, the mixture was placed in a dialysis membrane with a MW cut-off of 3,500 and dialyzed against deionized water for 48 h to remove excess reactants. After dialysis, the solution was diluted to 10 mM with respect to sPPO repeat unit by addition of deionized water. The pH was adjusted to 3 by addition of HCl. DMSO (20 wt. % with respect to EDOT) was added to the solution to provide secondary doping. The ratio of PEDOT:sPPO was controlled by changing the feed ratio of sPPO and EDOT. The PEDOT:sPPO ratio used for LbL assembly was 1:0.35 unless otherwise noted.

3.2.2 Layer-by-layer Assembly*:* A programmable ZEISS DS50 slide stainer was used to deposit films. Glass, ITO-coated glass, and silicon substrates were exposed to O_2 plasma in a Harrick PDC 32G plasma cleaner on high for 4 min to induce a negative surface charge. To construct LbL films, substrates were immersed in a PDAC solution (10 mM, pH 3) for 10 min, then in a series of two water rinse baths (pH 3) for 2 min each, followed by immersion into a stirred PEDOT:sPPO solution (10 mM, pH 3) for 10 min, then into a series of two water rinse baths (pH 3) for 2 min each. This process produced one bilayer (BL). The process was repeated until films had the desired thickness.

Tetralayer LbL films were constructed in a similar manner by immersing substrates in this series of baths: 10 min PDAC solution (10 mM, pH 3), 2 min x 2 water rinse baths (pH 3), 10 min sPPO solution (10 mM, salt and pH varied as noted in text), 2 min x 2 water rinse baths (pH 2), 10 min PDAC solution (10 mM, pH 3), 2 min x 2 water rinse baths (pH 3), 10 min

stirred PEDOT:sPPO solution (10 mM, pH 3), 2 min x 2 water rinse baths (pH 3). This process produced one tetralayer (TL).

Sprayed LBL films were deposited using identical solutions and rinse pH values. PDAC was sprayed for 3 s followed by spraying with water for 5 s. Then, PEDOT:sPPO was sprayed for 3 s followed with Mili-Q water for 5 s. The cycle was then repeated for the desired number of layer pairs.

3.2.3 Film Thickness: Thickness measurements were made by scoring films on flat substrates (glass or silicon) with a razor blade. The step height between the film and substrate was then measured with a Dektak 150 surface profiler. Reported thicknesses are the mean of 3 measurements on different areas of one film. Error bars displayed are the route-mean-squared roughness of the film.

3.2.4 Ionic Conductivity: Through-plane conductivity values were determined by performing impedance spectroscopy (Gamry PC4 Potentiostat/Galvanostat/ZRA) on films deposited on conductive substrates (ITO-coated glass) in a 3-electrode cell with the LbL coated ITO as the working electrode, a Pt mesh counter electrode, and a saturated Ag/AgCl reference electrode in 1 M H_2SO_4 electrolyte. Samples were conditioned by being held at 0 V referenced to Ag/AgCl for 30 min. Impedance was performed by sweeping the frequency from 100 kHz to 0.1 Hz, with a sinusoidal voltage amplitude of 10 mV. Impedance spectra were modeled using a dual rail transmission line equivalent circuit (see discussion in section 3.3.3). Impedance at elevated temperatures was achieved by placing the cell in an oil bath on an IKA stirrer hotplate with a temperature controller.

In-plane conductivity values were determined by performing impedance spectroscopy (Solartron 1260 impedance analyzer) on films deposited on glass (non-conducting) substrates with Pt wire electrodes in contact with the film surface. Impedance was performed by sweeping the frequency from 100 kHz to 0.1 Hz, with a sinusoidal voltage amplitude of 50 mV. Samples were enclosed in a humidity chamber and were allowed to equilibrate for 30 min prior to the measurements.

3.2.5 Ion Exchange Capacity: Films were assembled by dip LbL on polystyrene substrates. Post-assembly, but before drying the films were soaked in pH 1 water for 2 h to exchange the Ca^{2+} or Na^{+} ions for protons, then soaked in deionized water for 2 h to remove excess acid. Films were dried, and peeled off of the substrate. After weighing (samples varied from 3–4 mg), the free-standing films were soaked overnight in 1.5 mL of 1 M NaCl solution. 40 μL of phenolphthalein indicator solution (20x dilution of 0.5% w/v in 50% v/v EtOH:H_2O stock solution) was added with stirring. 4 mM aqueous NaOH solution was added dropwise from a pre-weighed filled syringe until a color change of the solution from clear to pale pink was observed. The syringe was then weighed again to determine the total amount of base added.

3.2.6 Electrical Conductivity: Electrical conductivity was measured on LbL films on glass substrates using a standard spring-loaded pressure contact Signatone S-302-4 four-point probe. The conductivity was calculated by $\sigma = (R_s \times t)^{-1}$ where R_s is sheet resistance and t is film thickness.

3.2.7 Other Analysis Ultraviolet/Visible Light spectroscopy was done on LbL samples assembled on plain glass substrates from 250 nm to 800 nm in wavelength using a Beckman Coulter DU 800 UV/Vis Spectrophotometer. Scanning electron microscopy characterization

was done using a JEOL 5910 SEM. A JEOL 5910 with a Bruker EDX system from the Center for Materials Science was used for sulfur mapping.

3.3 Results and Discussion

Motivated by the search for a multi-functional polymeric material for use as a membrane in a wireless solar-powered water splitting device, we investigated the use of LbL assembly for tuning the characteristics of membranes containing the recently reported mixed conducting composite PEDOT:sPPO.[4] While thin films of PEDOT:sPPO have excellent conductivity for this application, the water stability and visual transparence of these films need to be improved before they can be used in a working device. We hypothesized that the LbL process would modulate these properties by introducing electrostatic crosslinks to greatly improve the water stability, and by incorporating visually transparent polymer to increase the transparency of films at a given thickness. However, the LbL process was expected to reduce both the ionic and electronic conductivities of these films, so we undertook experiments to understand how the LbL process modifies each of these film properties.

3.3.1 PEDOT:sPPO in LbL films

In order to be incorporated in electrostatically assembled LbL films, solutions must have a zeta potential of at least $|\pm 30|$ mV. Zeta potential measurements of several ratios of PEDOT:sPPO show that all the solutions are sufficiently charged to act as the anionic layer in electrostatic self-assembled films (Figure 3.2a).

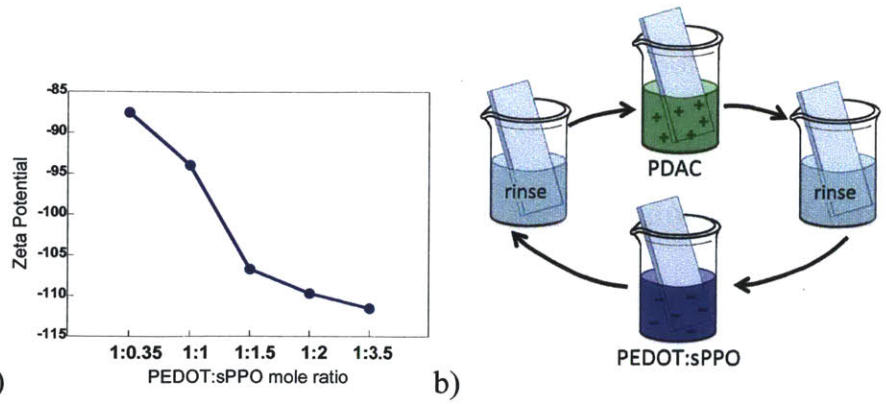

Figure 3.2. a) Zeta potential of PEDOT:sPPO solutions at various mole ratios. All solutions are sufficiently charged to act as the anionic layer in electrostatic self-assembled films. **b**) Schematic illustrating the LbL assembly process.

We based our choice of polymer materials on previous results so as to limit the number of initial variables for our experiments. Prior studies on optimizing the ionic conductivity of sPPO-containing LbL films found that PDAC was the best polycation to use.[5-6] So we elected to use PDAC for our studies of incorporating and modulating the properties of PEDOT:sPPO in LbL films. We chose to use solutions with a PEDOT:sPPO ratio of 1:0.35 for our initial studies because PEDOT was the only source of electrical conductivity in the films, whereas we had other options for increasing the composition ratio of sPPO in the films as discussed below in section 3.3.1.2

PEDOT itself is insoluble, making it difficult to process. The advantage of synthesizing it in an aqueous anionic polymer solution (besides the doping effect) is the resulting aqueous dispersion that is easy to process. Commercially available PEDOT:PSS contains proprietary additives that stabilize the dispersion in solution, giving these solutions a long shelf life. No stabilizing additives were used for the PEDOT:sPPO solutions in this study, hence they had a much shorter shelf life before aggregation reduced their ability to

form uniform LbL films. When solutions older than 4 weeks were used to deposit LbL films, the resulting films were composed largely of tens of microns scale aggregates (Figure 3.3). For all of the films reported in this work, the PEDOT:sPPO assembly solutions were less than 2 weeks old. Interestingly, PEDOT:sPPO solutions that had been sonicated to break up aggregates did not form films at all.

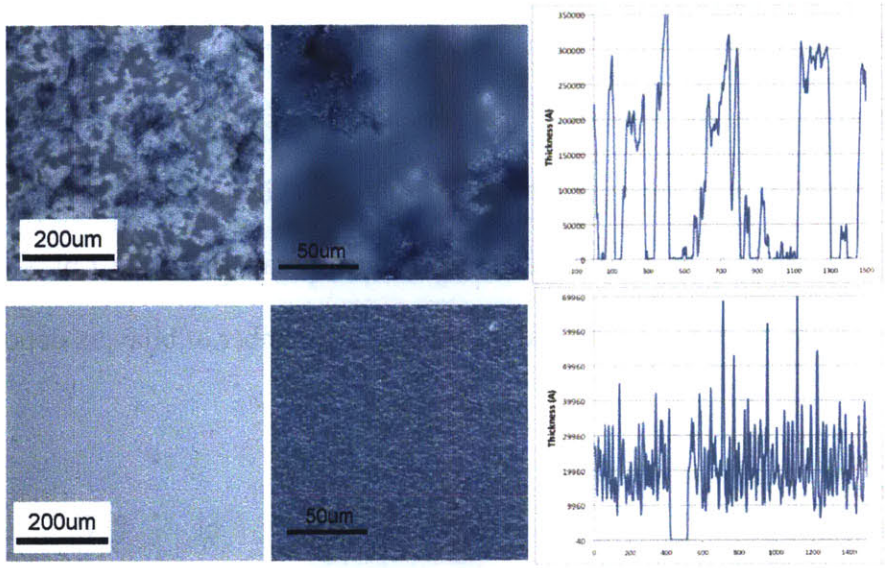

Figure 3.3. Optical microscope images of films assembled from PEDOT:sPPO solutions that were older than 4 weeks (top) are composed of tens of microns scale aggregates while aggregation is not visible on that scale in films composed of fresh solutions (bottom). Profilometry data reveals that films from old solutions are not continuous, with aggregates up to 30 μm in thickness next to regions that are only 100 nm thick. Films assembled from fresh solutions have a high roughness value, but are continuous.

3.3.1.1 Bilayer Architecture

Transparent mixed conducting polymer thin films were assembled by alternating immersion of a plasma treated glass substrate into an aqueous dispersion of the polymer

complex PEDOT:sPPO and into an aqueous PDAC solution (Figure 3.2b). Linear growth was observed with respect to the amount of polymer deposited per bilayer (Figure 3.4a). Furthermore, UV-Vis spectrophotometry was used to monitor the incorporation of PEDOT and sPPO into the films (Figure 3.4b). The peak at λ = 290 nm in the UV-Vis spectra is ascribed to the sPPO absorption, and the broad absorption from 400 nm to 800 nm corresponds to the PEDOT absorption, which extends to 3000 nm due to polaron and bipolaron absorption in the oxidized backbone. The absorbance of PEDOT and sPPO increases linearly with an increasing number of bilayers (Figure 3.4c). The absorbance data indicates that both PEDOT and sPPO are linearly incorporated into the LbL films, thus the film transparency can be easily controlled by altering the number of bilayers deposited.

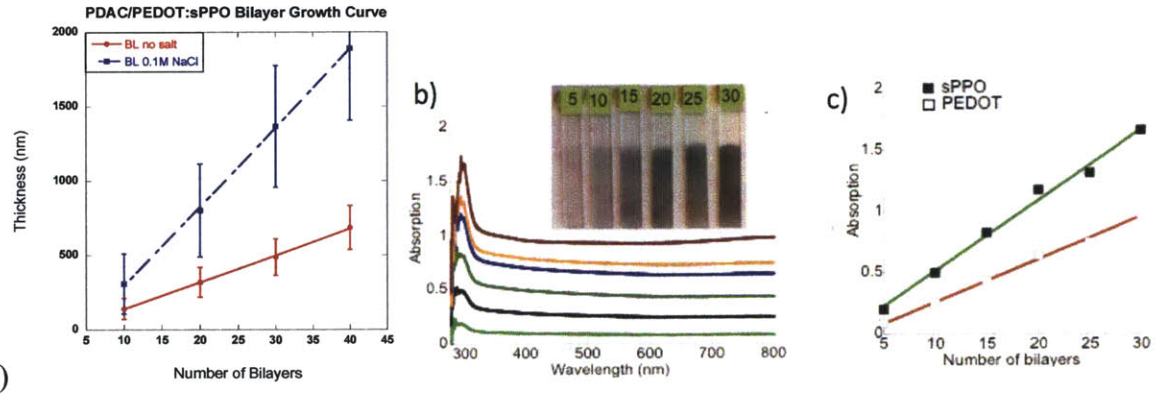

Figure 3.4. **a**) Film thickness as a function of the number of bilayers for PDAC/PEDOT:sPPO LbL films assembled with and without salt. The central point denotes the mean thickness and the error bars display the route mean squared roughness values. **b**) UV-Vis absorption spectra as a function of bilayer number. Inset is a photograph of LbL films coated on both sides of the glass. **c**) Peak height of sPPO and PEDOT absorptions in the UV-Vis spectrum plotted as a function of bilayer number.

Changing the assembly conditions of LbL films, especially the ionic strength of the assembly solutions, alters the growth profile and the ionic conductivity of the films due to the charge-screening effect of salt influencing the number of ionic crosslinks in the film.[7] In order to tune the ionic and electronic properties of our LbL films, films were assembled with 0.1 M NaCl in either the polycation or polyanion assembly bath. Adding salt to the PEDOT:sPPO solution resulted in precipitation of the polymer complex, so films could not be built. The films assembled with added NaCl in the PDAC solution showed linear growth with increasing number of bilayers, hence the growth rate of these LbL films can be readily tuned from 18 nm/bilayer without salt in assembly solutions to 53 nm/bilayer with 0.1 M NaCl into the PDAC solution (Figure 3.4a).

The bilayer films exhibited excellent stability in water: the films are stable in water under ambient conditions for more than eight months. In contrast, dropcast films of pure PEDOT:sPPO swell in water and break apart after ~ 12 h. This result is consistent with our hypothesis that electrostatic cross-linking in LbL films would improve the water stability of PEDOT:sPPO containing thin films.

3.3.1.2 Tetralayer Architecture

We hypothesized that increasing the composition ratio of sPPO in the films would be an important parameter in tuning the ionic conductivity of this series of materials. Two methods to increase the sPPO content and the number of free sulfonic acid sites (free meaning not bound in electrostatic cross-links) were investigated: a tetralayer architecture, and also the use of divalent salts to increase charge shielding during assembly. The first method incorporates layers of highly protonically conducting sPPO into each repeat unit of the film.

The mixed conducting PEDOT:sPPO is 1–2 orders of magnitude less protonically conducting than sPPO alone. The second method builds on the first by incorporating salts into the sPPO layers to make those layers thicker and to shield some of the sulfonic acid groups from being electrostatically bound to the quaternary amines of PDAC, leaving them free sites for proton-hopping. Each of these methods will be discussed in further detail below.

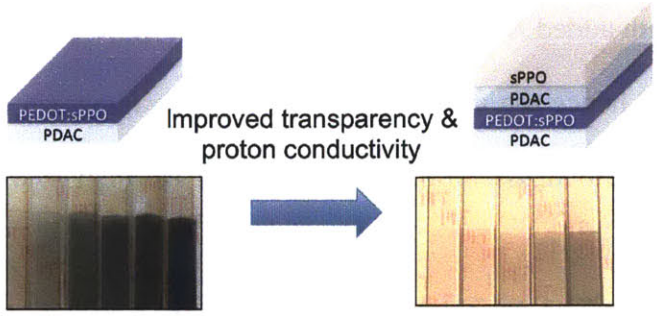

Figure 3.5. Schematic of bilayer and tetralayer film repeat units. Photographs of films of increasing numbers of layers showing the increased transparency of tetralayer films compared to bilayer films.

We use the nomenclature of tetralayer architecture to denote that the repeat unit of the LbL film has been changed from two layers to four layers. Every fourth layer, instead of a layer of PEDOT:sPPO, a layer of sPPO was deposited in its place (Figure 3.5). As evidenced by the photographs of bilayer (BL) and tetralayer (TL) films, the TL films are dramatically more transparent than the BL films, indicating less PEDOT concentration in the films. (Both PDAC and sPPO are transparent in the visible range.) UV-Vis absorption spectra indicate an increase in sPPO concentration for BL and TL films of similar thickness (Figure 3.6).

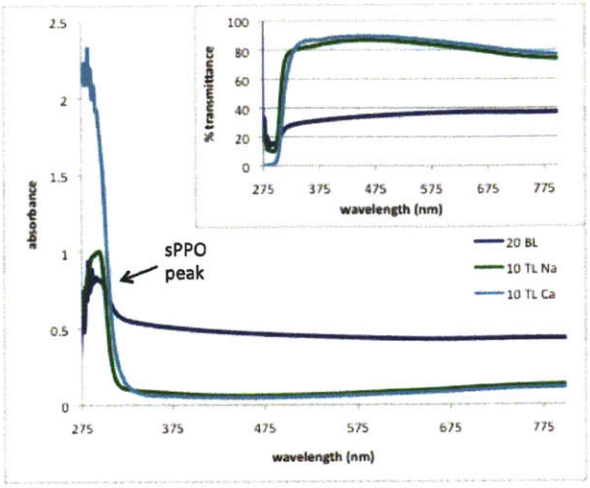

Figure 3.6. UV-vis spectrum of ~1.1 μm thick films (~550 nm coated on both sides of a glass slide) while wet. The tetralayer films are far more transparent than the bilayer films, exhibiting 80% transmittance compared to < 40%. The absorbance data shows that the films assembled with $CaCl_2$ incorporate more sPPO per TL than films assembled with NaCl.

Building upon the tetralayer architecture, we wanted to increase the amount of sPPO in each layer. To further increase the composition ratio of sPPO, we added salts to the sPPO solution. Simply increasing the concentration of one polymer bath over another does not result in an increase of that polymer in the overall LbL film because excess unbound polymer beyond what is needed to reverse the surface charge is removed during rinse steps.[8] Instead, the composition ratio can be tuned by changing the ionic strength or pH of the assembly solutions, which changes the effective charge density along the polymer chains by either salt shielding the charges from each other in the case of strong polyelectrolytes, or by protonation/deprotonation in the case of weak polyelectrolytes.[5, 9] With a lower effective charge density and thus less self-repulsion, the polymer chains deposit in a "loopy" morphology (as opposed to a stretched out morphology due to self-repulsion) and thus require more polymer to effectively reverse the surface charge.

Protonic conductivity (σ_H) is dependent on both the number of free protons (n_H) and the proton mobility (μ_H) as shown in this equation: $\sigma_H = n_H \cdot e \cdot \mu_H$, where e is the electronic charge of a proton. The use of divalent salts in assembly of PDAC/sPPO films was shown to increase the protonic conductivity of these films by a factor of 5.[10] This dramatic improvement in conductivity was shown to be caused by an increase in the composition ratio of sPPO in the films (hence increasing the number of free protons), and by a reduction in the energy of activation for proton conduction (thus improving the proton mobility).[10] The improvement in mobility is believed to be due to ion bridging between sulfonic acid groups during film formation resulting in a more connected path for proton hopping. After assembly, the films were soaked in 0.1 M HCl, so each Ca^{2+} ion that had been incorporated into the film was replaced with 2 protons. In order to understand whether the use of a divalent salt would have similar salutary effects on the conductivity of the TL films, we assembled films with either NaCl or $CaCl_2$ at a variety of concentrations in the sPPO solution.

The TL films regardless of salt condition exhibited a slow growth induction period for the first 10 TL, followed by linear growth up to ~25 TL, and superlinear growth at 30 TL (Figure 3.7). By "superlinear" growth we mean that there is a sudden large jump in film thickness that is likely due to interdiffusion of polymer chains into the bulk of the film rather than only depositing on the surface of the film. Interdiffusion is more often observed with weak polyelectrolytes, but has also been observed in strong polyelectrolyte systems with high salt concentrations. The thickness per TL in the linear region increased with the addition of NaCl and increased further with the addition of $CaCl_2$ (Table 3.1). The lone exception is with films assembled at pH 2 with 0.75 M $CaCl_2$, indicating that eventually at very high divalent salt concentrations there is an inhibitory effect on film growth.

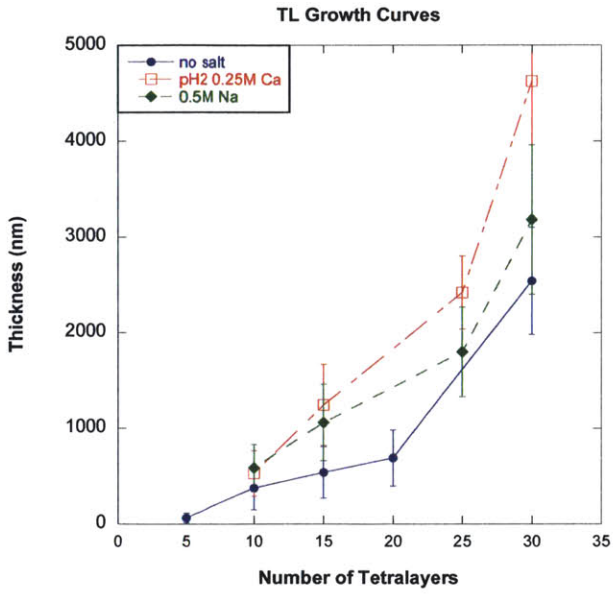

Figure 3.7. Growth curves for tetralayer films. The center marks show the mean thickness and the error bars represent the route mean squared roughness.

The TL films all exhibited high surface roughness (Figure 3.7), with the $CaCl_2$ films having the highest roughness values, as was also seen with PDAC/sPPO films assembled with Ca. The surface roughness results in increased light scattering, making the Ca TL films look less transparent when dry. Since the solar water-splitting application that inspired this work calls for a visually transparent membrane that will be immersed in water, the UV-vis measurements were taken on wet films to reduce the scattering effect. Use of an integrating sphere for UV-vis measurements on the dry films would be a valuable method to separate the absorption profile of these films from the effect of light scattering. The UV-vis spectra of 1.1 μm thick TL films assembled with Ca^{2+} and Na^{+} show that they both have excellent transmittance of ~80% when wet (Figure 3.6). The absorbance data indicates that the Ca films have a higher proportion of sPPO, consistent with the effect Ca salts have on PDAC/sPPO films.

PDAC salt	PEDOT:sPPO mole ratio	sPPO		Thickness at 10 BL/TL	Growth in linear region	Electrical Conductivity (mS/cm)
		pH	salt			
0.1 M NaCl	1:0.35	N/A		309 nm	53 nm/BL	350
no salt		N/A		142 nm	18 nm/BL	700
		2	no salt	374 nm	31 nm/TL	387
		2	0.25 M NaCl	555 nm	85 nm/TL	141
		2	0.5 M NaCl	584 nm	80 nm/TL	179
		2	0.25 M $CaCl_2$	525 nm	125 nm/TL	45
		2	0.5 M $CaCl_2$	595 nm	106 nm/TL	98
		2	0.75 M $CaCl_2$	493 nm	22 nm/TL	73
		1	0.5 M $CaCl_2$	513 nm	104 nm/TL	43
		1	0.75 M $CaCl_2$	466 nm	98 nm/TL	74
	1:2	2	0.5 M $CaCl_2$	N/A	64 nm/TL	0.38

Table 3.1. Film growth and conductivity characteristics for a variety of film architectures.

3.3.2 Electrical Properties of LbL Films

Incorporating PEDOT:sPPO into LbL films was expected to impact the electrical conductivity compared to the pure material due to the addition of electrically insulating PDAC, which may disrupt the pathways for electron or hole conduction. We investigated the magnitude of the change in conductivity through the use of a four-point probe. Electrical conductivities are listed in Table 3.1. Compared with spin-cast PEDOT:sPPO films, the BL films showed an order of magnitude lower electrical conductivity, which may be attributed to the incorporation of insulating PDAC effectively "diluting" or lowering the current density of the film.

Interestingly, with increasing number of bilayers, the electrical conductivity first increased, then reached a plateau. At 5 BL no electrical conductivity can be detected, at 10 BL the electrical conductivity is 94 mS/cm, but by 15 BL the electrical conductivity reaches a plateau of 700 mS/cm. This observation is consistent with the observations made by Durstock,[11] which they claim are due to structural changes in the films with increasing number of bilayers. But no further study of these structural changes has been conducted.

To understand how the film morphology changes as the films grow and how the morphology affects the electrical conductivity, TEM and SEM were used to investigate the morphology of the LbL films. TEM images revealed that PEDOT:sPPO pre-aggregated and formed nanofibril structures (Figure 3.8a); this fibrillar structure facilitates charge transport in the films. Upon LbL assembly of PEDOT:sPPO with PDAC, at 5 BL only isolated nanofibils were formed, hence no electrical conductivity was detected. At 10 BL, more fibrils formed on the films and these fibrils start to connect to each other and form electron percolation pathways, thus the film showed low conductivity. By 15 BL, the fibrils form 3-D web-like structures, thus creating an electron percolation pathway, resulting in excellent electrical conductivity. To confirm that these fibrillar structures are PEDOT:sPPO, SEM-EDS was further conducted. EDS analysis revealed that the fibrillar network contains sulfur, which is only present in PEDOT:sPPO in these films (Figure 3.8e).

It is believed that the dipping LbL process is thermodynamically controlled, hence PEDOT:sPPO can rearrange and form nanofibrillar structures, which facilitate the charge percolation. However, in films built using a much faster spray LbL process (deposition takes seconds v. 10 min for dipping), no fibril structures were observed (Figure 3.8f), and these films did not show any electrical conductivity. The lack of fibril structures in the sprayed LbL films is likely due to kinetic control of the spray LbL film morphology, hence PEDOT:sPPO could not rearrange in the short time scale of the spraying process to form a percolative network for electronic conduction. Another possibility is that the fibril structures formed in solution prior to spraying, but were unable to stick to the substrate. The sprayed films were very thin compared to dipped films, indicating that poor adherence to the substrate could be involved. Carbon nanotubes were found to be poor at adhering to flat substrates in spray LbL

due to their dimensions, but changes to the spray protocol such as using a porous substrate with applied vacuum resulted in good adherence and the formation of thick films.[12] Perhaps similar techniques could result in sprayed PEDOT:sPPO LbL films with morphologies that promote conductivity.

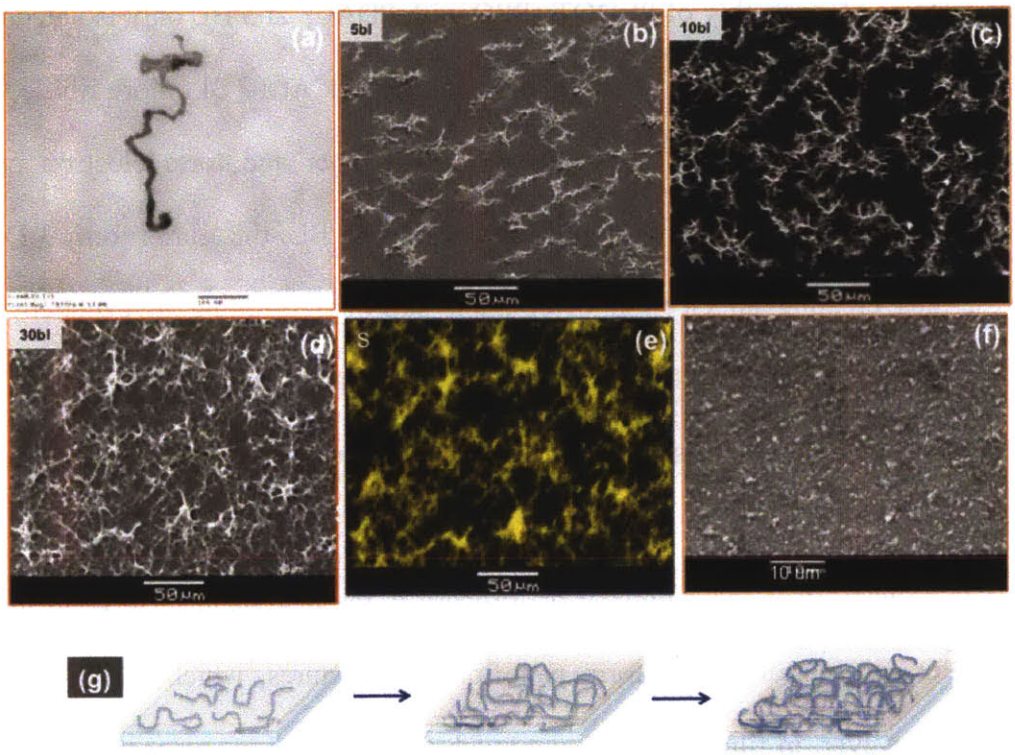

Figure 3.8. **a**) TEM image of pre-aggregated PEDOT:sPPO. SEM images of **b**) 5 BL, **c**) 10 BL, and **d**) 30 BL PDAC/PEDOT:sPPO LbL films. **e**) SEM-EDS sulfur mapping of the 30 BL film. **f**) SEM image showing the morphology of a sprayed PDAC/PEDOT:sPPO LbL film. **g**) Schematic illustrating how the morphology changes with increasing number of bilayers.

Cyclic voltammetry was conducted to further understand the electrochemical behavior of these films (Figure 3.9). The increase in the current with increasing film thickness, and the retention of electroactivity despite insertion of the insulating PDAC layer, indicate that

PEDOT is interpenetrating between the layers throughout the film. For 5 BL films, there is very low current response, indicating that the PEDOT:sPPO regions in the film are non-continuous. However, 15 BL films showed a dramatic increase in current response, indicating PEDOT:sPPO formed a continuous network. This result is in good agreement with the morphology changes observed in SEM.

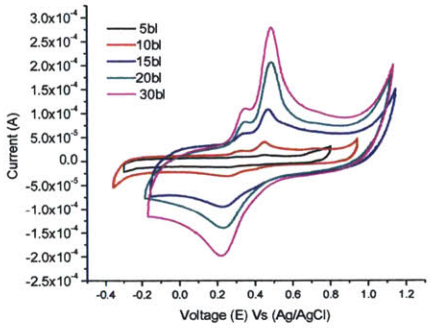

Figure 3.9. Cyclic voltammagrams of LbL films at a scan rate of 25 mV/s showed a dramatic increase in current between the 10 and 15 BL films indicating a continuous network of electrically conducting pathways.

Though PEDOT was only incorporated every 4th layer in the TL films, these films still exhibited electrical conductivity, indicating that the PEDOT:sPPO nanofibrils are still forming a percolative network throughout the films. Though we often draw LbL films as stratified layers for illustrative purposes, the layers are generally interpenetrating with only "fuzzy" boundaries between them. Previous studies of LbL film composition have indicated that this interpenetration spans four layers, consistent with these results.[13] As expected, the increase in composition ratio of electrically insulating sPPO in the TL films was inversely proportional to the electrical conductivity: the electrical conductivity was roughly halved going from BL to TL films, and halved again going from TL with no salt to TL with NaCl.

The TL films assembled with $CaCl_2$ were less electrically conductive than the Na films, but there was no clear relationship between conductivity and pH or salt concentration amongst the Ca films.

All of the films discussed thus far were composed of PEDOT:sPPO in a 1:0.35 ratio. In an attempt to probe the limits of PEDOT composition ratio while still retaining electrical conductivity, films were assembled using 1:2 PEDOT:sPPO. Without salt, these films grew very slowly, only 4 nm/TL, and were electrically insulating, but with 0.5 M $CaCl_2$, the films grew at 64 nm/TL and had a very low electrical conductivity of 0.38 mS/cm.

Films in the superlinear thickness range had much lower electrical conductivities than the same film architecture in the linear growth range. This ~10 fold drop in conductivity can likely be explained by a combination of interdiffusing polymer chains interfering with the interpenetration and contact between the PEDOT:sPPO nanofibrils across layers and by further dilution of the current density of the films.

Salt Conditions in sPPO	30 TL Thickness (μm)	Roughness (μm)	Electrical Conductivity (mS/cm)
No salt	2.54	0.56	12
0.5 M NaCl	3.18	0.78	4
0.25 M $CaCl_2$	4.62	1.40	2

Table 3.2. Superlinear range film thickness and electrical conductivity.

3.3.3 Impedance Spectroscopy of LbL Films

Measuring conductivity in ultrathin films can be difficult because resistance is proportional to the distance travelled, so in the case of highly conducting ultrathin films the resistance through the plane of the film will be very low. Prior studies of the ionic conductivity of PDAC/sPPO proved that the conductivity in this material is isotropic, and thus for very thin films, impedance spectra were measured using electrodes in an in-plane

geometry, allowing the distance between the electrodes to be increased so that the impedance would be in a measurable range.[5-6] We initially began our studies of ionic conductivity in mixed conducting LbL films by using the same experimental set up we had used for ionically conducting but electrically insulating LbL films (Figure 3.9a). We expected that the spectra plotted in the complex plane (Nyquist plot) would consist of two semicircles, corresponding to the two different time constants for the movement of the different charged species: electrons (or holes), and protons. Instead we observed only one semicircle, and the low frequency intercept with the real axis corresponded to the resistance that would be expected based on the electrical conductivity of the sample that had been independently measured via 4-point probe. We reasoned that the electrical conductivity of the sample must be so much greater than the ionic conductivity that it was just shorting the measurement, and thus we would not be able to observe ionic conductivity in an in-plane configuration with both electrodes in contact with the film surface. Thus we switched to performing through-plane impedance measurements in an electrochemical cell with LbL films on ITO-coated glass slides as the working electrode, Ag/AgCl as a reference electrode, and a Pt mesh counter electrode in 0.5–1 M H_2SO_4 electrolyte at room temperature.

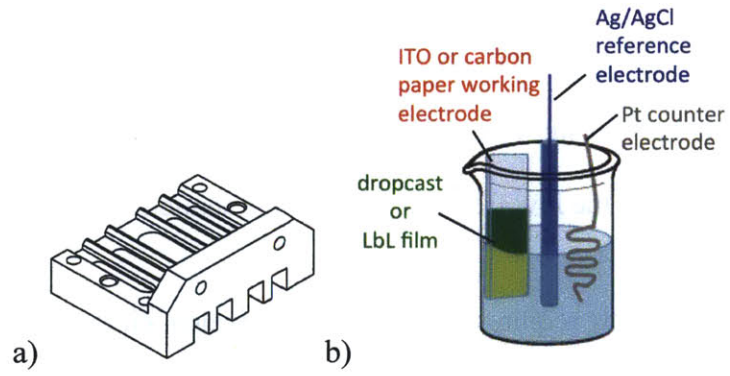

Figure 3.9. **a**) Electrode consisting of plastic holder with platinum wires held at fixed distances. This electrode was clamped in contact with films built on glass substrates for in-

plane impedance measurements. **b**) Electrochemical cell for measuring through-plane impedance of films built on conducting substrates.

The shape of the impedance spectrum plotted in the complex plane provides insight into possible mechanisms or governing phenomena for conductivity.[14] A perfect semicircle indicates a single activation-energy-controlled process, while multiple peaks indicate more than one time constant is needed to describe the process, and a depressed semicircle can be observed in more complex scenarios (e.g. multiple processes with partially overlapping time constants).[14] Note that analysing the shape of Nyquist plots requires the data to be plotted with orthonormal axes. Straightforward analysis can be performed by graphically interpreting the spectrum, and more sophisticated analyses can be performed using computer modelling to replicate the spectrum.

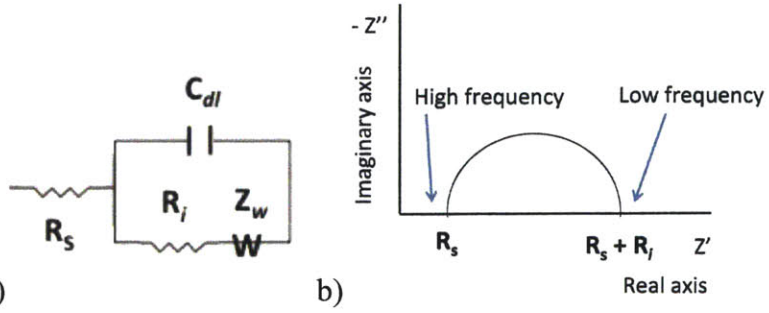

Figure 3.10. **a**) Randles circuit model used for interpreting simple impedance spectra. **b**) Complex plane (Nyquist) plot result from Randles circuit. The Warburg element, if observed, will appear as a 45° line from the low frequency end of the semicircle.

Impedance spectroscopy requires the use of an equivalent circuit model to interpret the data. For ion conducting polymer films, interpretation using the Randles circuit is well established (Figure 3.10). The Randles circuit consists of a resistor representing electrolyte resistance (or parasitic lead resistance if not using an electrolyte) in series with a parallel

combination of a capacitor representing the bulk polarization of the film and a resistor representing the resistance to ion movement in the film. Also included is a Warburg element representing the diffusion-limited regime. Often the capacitor is replaced with a constant phase element to better model the non-ideality of real systems. When plotted in the complex plane, the Randles circuit provides a spectrum that looks like a semicircle where the high frequency intercept with the real axis corresponds to the series resistance (R_s), and the diameter of the semicircle corresponds to the ionic resistance (R_i) (Figure 3.10).

The appropriate choice of equivalent circuit to use for intrinsically conducting polymers has been subject to much debate. Pickup and coworkers have used a finite transmission line model consisting of a line of resistors representing ionic resistance in parallel with a line of resistors representing electronic resistance to interpret spectra from many conducting polymers and mixed conducting composites.[15] Also included are capacitors in between the two rails representing the polarization of the polymer. They have used this model to interpret spectra from PEDOT:PSS,[15] which we expected to behave similarly to PEDOT:sPPO used in this work. The transmission line model predicts a 45° region at high frequency, reflecting the ion and electron migration within the film, followed by a 90° region at low frequency, corresponding to the capacitance response of the film. They posit that the transmission line model is appropriate for these systems as it represents the boundaries between charges traveling in electrolyte in the pores of the film and charges moving in the polymer phase. The data for dropcast films of PEDOT:sPPO were in good agreement with the predictions of the finite transmission line model.[4] Using this model for films with high electrical conductivity, the electrical resistance is negligible and the ionic resistance can be calculated according to $R_i = 3\left(Z'_{low} - Z'_{high}\right)$; where Z'_{low} is the real axis intercept of a

linear regression of the 90° region and Z'_{high} is the real axis intercept of the 45° region. For films where the ionic and electronic resistances are closer to each other and hence neither one is negligible, the following equations can be used:

$$Z'_{low} = R_{cell} + \frac{R_\Sigma}{3}$$

$$Z'_{high} = R_{cell} + R_\infty$$

where R_{cell} is the resistance of the cell with a bare electrode and

$$R_\Sigma = R_e + R_i$$

$$\frac{1}{R_\infty} = \frac{1}{R_e} + \frac{1}{R_i}$$

The conductivity can be calculated by $\sigma = \frac{\ell}{R_i A}$ where ℓ is equal to the film thickness for through plane measurements.

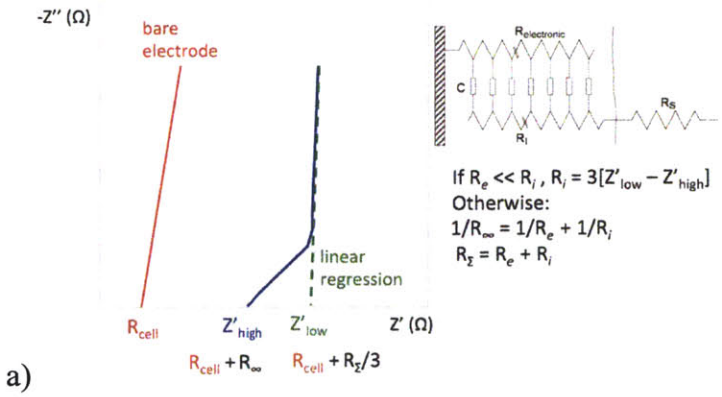

a)

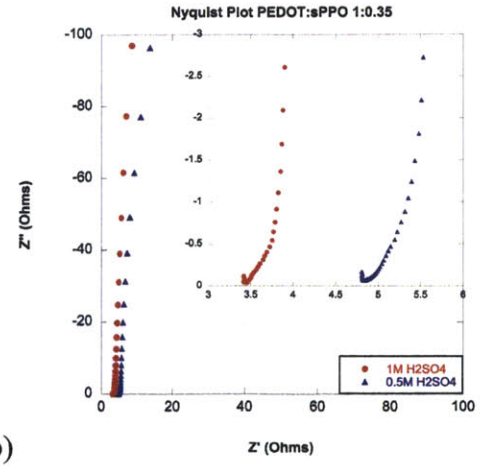

b)

Figure 3.11. **a**) Transmission line equivalent circuit and the expected Nyquist plot. **b**)

Impedance spectra of PEDOT:sPPO films are in good agreement with the model.

Ion conduction in sulfonated polymers like sPPO is generally accepted to proceed via the Grotthuss mechanism, wherein protons hop between sulfonate groups facilitated by the hydrogen bond network in water (Figure 3.12). Hence each individual proton does not need to move very far, rather covalent bonds to protons are formed and broken along the hydrogen bonding network of water resulting in proton conduction. Since water facilitates this mechanism, the proton conductivity in sPPO-containing films is dependent on the relative humidity when measured in air; but when measured in solution, it is dependent on the electrolyte concentration (since that affects the number of charge carriers available) The conductivity of pristine PEDOT:sPPO films is twice as high in 1 M H_2SO_4 as in 0.5M H_2SO_4. For the water-splitting device membrane application that motivated this study, the target minimum conductivity is 0.1 mS/cm for a film less than 10 μm thick.[2] Hence impedance spectroscopy was performed on the PEDOT:sPPO containing LbL films in 1 M H_2SO_4 electrolyte so as to maximize the conductivity in an attempt to find films with conductivities close to or above the desired minimum of 0.1 mS/cm.

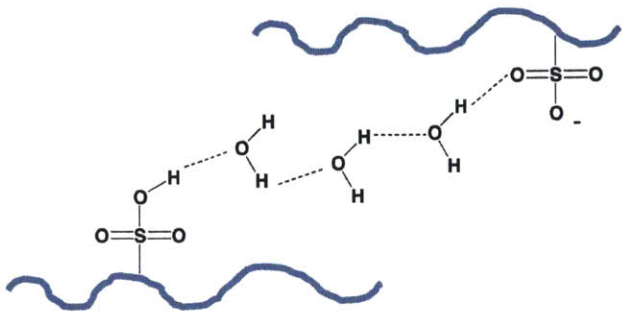

Figure 3.12. Cartoon illustrating the Grotthuss mechanism of proton hopping.

We expected the PEDOT:sPPO containing LbL films to exhibit similar spectra to the pristine material, anticipating that the same equivalent circuit could be used. At lower numbers of bilayers in 1 M H_2SO_4, the spectra looked as though they might follow the model, but the 45° region was small and hard to discern. Unlike the dropcast films of PEDOT:sPPO, which could be made as thick as desired, the LbL films were extremely thin, so the resistances we were trying to measure were very small. The conductivities calculated by this method are listed in Table 3.3. The ionic conductivity follows an inverse trend as the electrical conductivity: the ionic conductivity roughly doubles when going from BL to TL, and doubles again when going from TL with no salt to TL assembled with NaCl in the sPPO bath, and doubles again when assembled with $CaCl_2$ in the sPPO bath.

PDAC salt	PEDOT:sPPO mole ratio	sPPO		Electrical Conductivity (mS/cm)	Ionic Conductivity (mS/cm)
		pH	salt		
0.1 M NaCl	1:0.35	N/A		350	0.006
no salt		N/A		700	0.0048
		2	no salt	387	0.009
		2	0.25 M NaCl	141	0.03
		2	0.5 M NaCl	179	0.03
		2	0.25 M $CaCl_2$	45	0.08
		2	0.5 M $CaCl_2$	98	0.07
		2	0.75 M $CaCl_2$	73	0.04
		1	0.5 M $CaCl_2$	43	0.05
		1	0.75 M $CaCl_2$	74	0.06
	1:2	2	0.5 M $CaCl_2$	0.38	62 at 98% RH

Table 3.3. Ionic conductivities of PEDOT:sPPO containing LbL films.

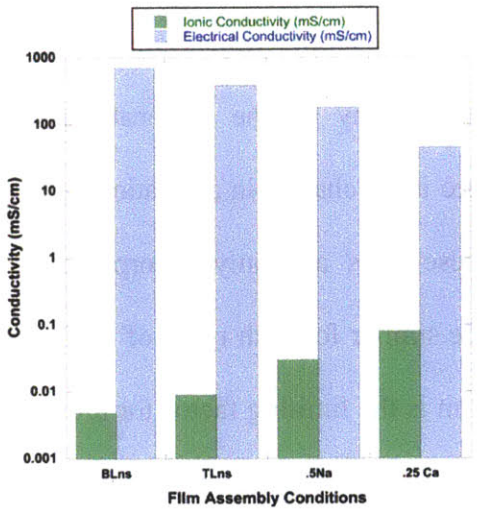

Figure 3.13. Chart illustrating how film ionic and electrical conductivity can be tuned at the expense of one another by changing film assembly conditons. Note the conductivity is displayed on a log scale.

The TL films assembled with 1:2 PEDOT:sPPO and $CaCl_2$ were measured using the in-plane impedance set-up in a humidity chamber and were only 10 mS/cm lower than PDAC/sPPO films. This fact, along with their white color and very low electrical conductivity, indicates that very little PEDOT was incorporated into these films.

In order to determine whether the improvement in ionic conductivity provided by addition of Ca^{2+} salts was due to a change in proton mobility as was seen in the case of proton conducting PDAC/sPPO films, we recorded impedance spectra at various temperatures. The change in ionic conductivity as a function of temperature can be related to the activation energy for proton conduction by the Arrhenius equation $\sigma = \sigma_o \exp\left(\frac{-E_a}{RT}\right)$, where σ is the ionic conductivity, σ_o is a pre-exponential factor, E_a is the activation energy, R is the Boltzman constant, and T is temperature in Kelvin. The data and resulting activation energies are displayed in Figure 3.14. The activation energy for proton conduction in the TL films is

much higher than for PEDOT:sPPO alone, which is expected because the TL films contain insulating PDAC material and many of the sulfonate groups of sPPO are tied up in electrostatic interactions. There is no change in activation energy for the TL films assembled with Ca^{2+} or Na^{+} salts. These salts are only incorporated in the sPPO layers, so the PEDOT:sPPO layers should be similar for both types of films. Perhaps movement through the PEDOT:sPPO layers of the film is the limiting factor for proton mobility in these films, hence the addition of salt in the sPPO layers had no effect on the mobility.

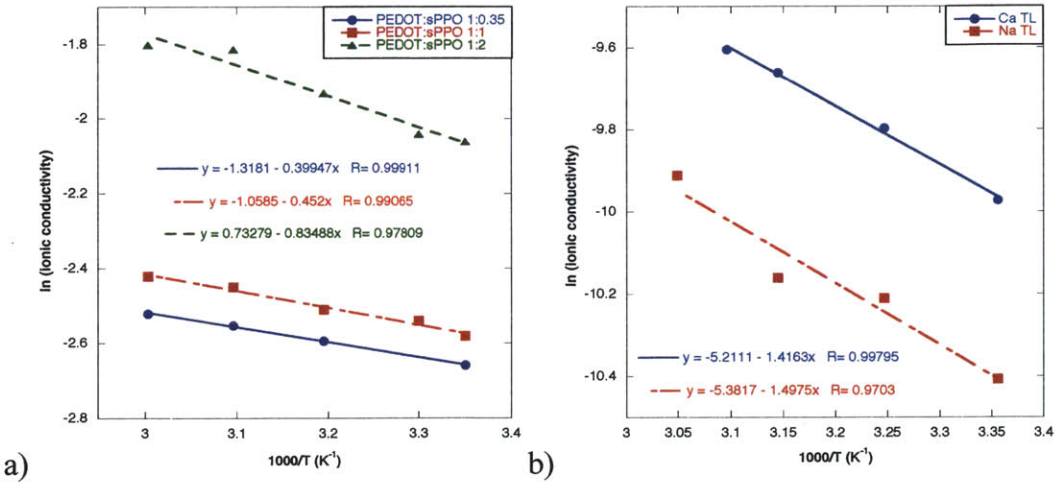

Material	1:2 PEDOT:sPPO	1:1 PEDOT:sPPO	1:0.35 PEDOT:sPPO	TL: PDAC/ sPPO ($CaCl_2$) PEDOT:sPPO	TL: PDAC/ sPPO (NaCl) PEDOT:sPPO
E_a (kJ/mol)	6.94	3.76	3.32	12	12

Figure 3.14. Plots of ln(ionic conductivity) vs. 1000/(temperature) for **a**) various ratios of PEDOT:sPPO and for **b**) TL LbL films assembled with either $CaCl_2$ or NaCl. **c**) Calculated activation energies for proton conduction.

Unexpectedly, once we looked at thicker BL films in 0.5 M H_2SO_4, (hence the impedance should be higher) the shape of the Nyquist plots for the PDAC/PEDOT:sPPO 40 bilayer films exhibited a semicircle at high frequency that trails off into a capacitive region at low frequencies (Figure 3.15). Pickup and coworkers mention one instance of a similar

looking spectrum of a mixed conducting polymer film, but did not provide an interpretation of this result as it did not follow the transmission line model.[16] It is not clear why the LbL film would not resemble the behavior of the pure material, since the added material is insulating, but perhaps it is a morphological change, such as the LbL films being less porous than PEDOT:sPPO alone.

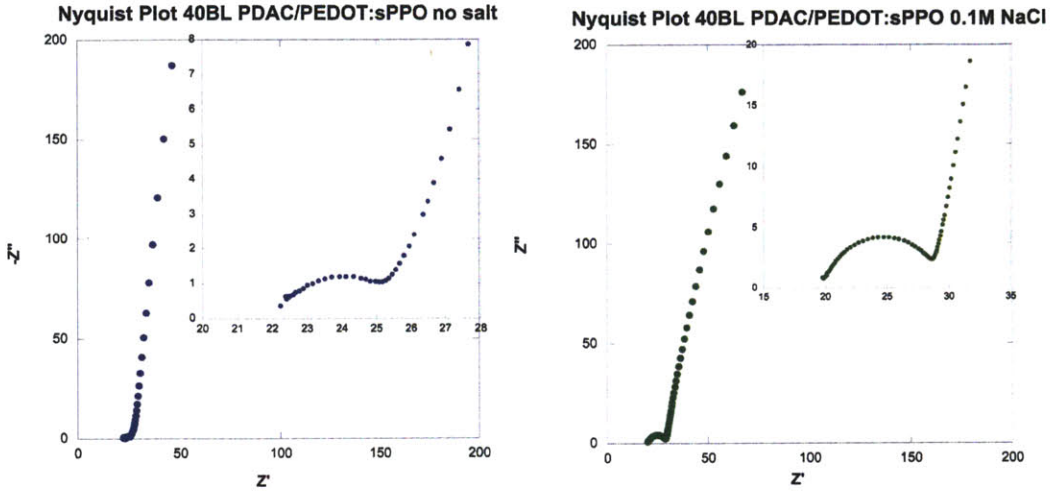

Figure 3.15. Nyquist plots for 40 BL LbL films in 0.5 M H2SO4 exhibit a semicircle at high frequencies and a capacitive response at low frequencies.

As a first approximation, the simplest equivalent circuit that we can propose for the bilayer LbL films is a linear combination of the equivalent circuits for the constituent materials. The equivalent circuit used to model PDAC/sPPO films is the Randles circuit discussed above. The equivalent circuit we propose for PEDOT is also simply a constant phase element in parallel with a resistor, which has been used for pure conducting polymers such as P3HT.[1c] Based on the morphology observed in the SEM and the 4 point probe and CV results, we expect that these bilayer LbL films contain continuous pathways for both ion and electron or hole conduction, as the sPPO and PEDOT are bound together throughout the film,

and the PEDOT forms a percolative network for electrical conduction. Thus a parallel combination of the constituent circuits seems to be a reasonable approximation, and combined with a resistor in series to represent IR loss through the electrolyte gives us the circuit shown in Figure 3.16.[17] This equivalent circuit model predicts a Nyquist plot containing two semicircles, but the bilayer film spectra only exhibit one. Based on the electrical conductivity measured by 4-point probe, the electrical resistance in these films should be on the order of 10^{-7} Ω, which is much too small to observe in this experimental set-up and is negligible compared to the ionic resistance. Thus a reasonable approximation is simply using the circuit used for PDAC/sPPO. Under that model, the ionic resistance is given by the diameter of the semicircle along the x-axis, and the corresponding conductivities are 1 x 10^{-2} and 1.5 x 10^{-2} mS/cm for the no salt and 0.1 M NaCl bilayer films respectively. This is an order of magnitude larger than the conductivities determined using the transmission line model.

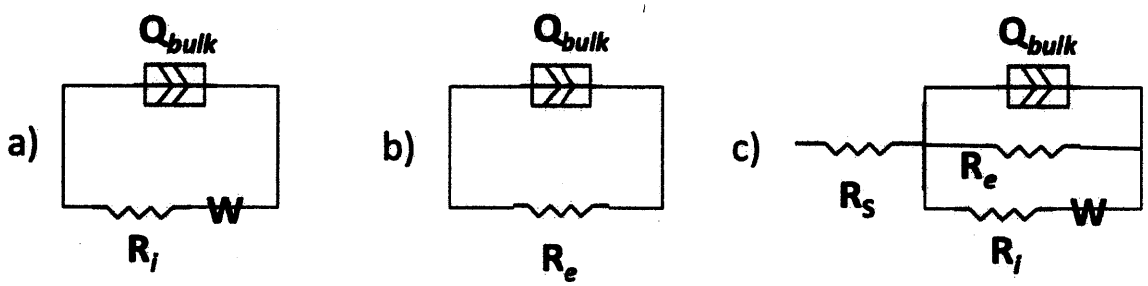

Figure 3.16. Equivalent circuit models for **a)** ion conducting film, **b)** electronically conducting film, and **c)** parallel combination of ion and electronically conducting circuits. R_s is solution resistance in the electrolyte, Q_{bulk} is the capacitance of the constant phase element, R_i and R_e are the ionic and electrical resistance, and W is the Warburg element.

The ionic conductivities of the bilayer LbL films determined from these later spectra and of the TL films are two to three orders of magnitude lower than those of pure

PEDOT:sPPO films, which are on the order of 1-10 mS/cm depending on the component ratio. This loss in conductivity is likely due to the higher cross-link density resulting in a dramatically decreased number of free mobile protons associated with the sulfonic acid groups. A similar effect is seen when comparing the ionic conductivities of pristine sPPO (~400–600 mS/cm depending on sulfonation %) to PDAC/sPPO LbL films (varies from 1–70 mS/cm depending on salt levels in assembly solutions). For the water-splitting device membrane application that motivated this study the target minimum conductivity is 0.1 mS/cm for a film less than 10 μm thick.[2] The LbL film conductivities are one order of magnitude too low to be useful for this application.

The unexpected spectra for the thicker BL films caused us to question our interpretation of the earlier LbL film spectra. Likely what we interpreted as the very small 45° region was actually noise or an artifact of the spectrum transitioning to 90°. We have seen when measuring the proton conductivity of Nafion (a commercially available proton exchange membrane) that with very high conductivity, the expected semicircular region of the spectrum does not appear and instead only a capacitive region is observed, where the intercept with the real axis is taken as the ionic resistance. However in this case, the intercept with the real axis would be equivalent to the solution resistance of the cell plus the ionic resistance of the film. Unfortunately the variability in the solution resistance of the cell used turned out to be larger than the resistances we would expect from the films. Our recommendation to clarify the conductivity values for these films is to repeat these measurements in a different cell with much smaller and more carefully controlled distances between the electrodes. Alternatively, it might be preferable to eliminate the use of solution entirely and to instead use a metallic top contact for the surface of the films such as coating them with evaporated gold. However, we

believe that the ionic conductivities listed in Table 3.3 as determined by the transmission line model should be considered a lower limit for the conductivity of these films based on the BL film results.

3.3.4 Ionic Conductivity of Tetralayer Films in the Superlinear Growth Regime

Reasoning that the 30 TL films, which were much thicker and corresponded to the superlinear growth regime, would shed more light on the ionic conductivities of these films, we measured them using the in-plane electrodes typically used for ion conducting (as opposed to mixed conducting) films. The impedance of these films was measured at 30, 60, 80, and 98 percent relative humidity. At low humidity, the ionic conductivity should be very low, but is expected to increase exponentially as the humidity increases based on the behavior of PDAC/sPPO films. The films assembled with NaCl and with no salt had spectra that looked like depressed semicircles at all of the humidity conditions, indicating that the time constants for electron and proton conduction in these films were somewhat overlapping so the ionic conductivities could not be determined. However, the spectra for the 30 TL films assembled with $CaCl_2$ resembled a depressed semicircle at 30% RH that slowly resolved into two separate semicircles as the humidity increased (Figure 3.17). We chose to model the spectrum at 98% RH using the equivalent circuit shown in Figure 3.16c based on the same reasoning as used for the BL film spectra. However in this case the electronic resistance is not negligible. This equivalent circuit model predicts that the first intercept with the real axis will be equal to a parallel combination of the ionic and electronic resistances, and the second (or extrapolated) intercept with the real axis is equal to the electronic resistance. Based on the 4-point probe measurements, the extrapolated 2^{nd} intercept was equal to the electronic

resistance. Thus the ionic conductivity of this film was calculated to be 4 mS/cm at 98% RH. This film surpasses the stated conductivity goal for the solar water-splitting device membrane of 0.1 mS/cm.

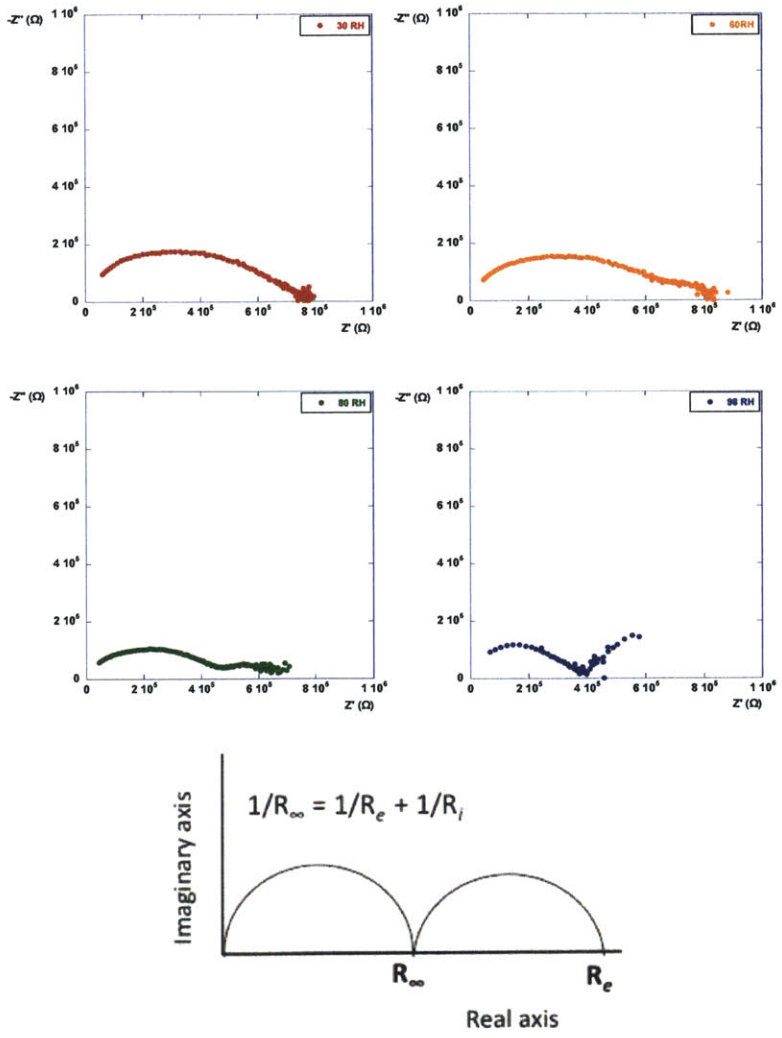

Figure 3.17. **a**) Complex plane plots of impedance spectra for a 30 TL film assembled with $CaCl_2$ at 30, 60, 80, and 98% RH. The calculated ionic conductivity of this film was 4 mS/cm at 98% RH. **b**) The complex impedance plot predicted by the circuit model used.

To further understand the nature of the conductivity differences between different film assembly conditions, we measured the proton exchange capacity of the 30 TL films assembled with NaCl and $CaCl_2$. The ion exchange capacity is a measure of the number of free protons in a film, and a standard metric for characterizing proton exchange membranes. PDAC/sPPO/PDAC/PEDOT:sPPO TL films were assembled on polystyrene substrates, and after assembly they were immersed in pH 1 water for 2 h to exchange all of the Ca^{2+} or Na^{+} ions with protons, followed by immersion in Milli-Q deionized water for 2 h to remove any excess acid. Once dry, the films were peeled off the substrate to generate free-standing films. These films were soaked overnight in 1 M NaCl to exchange all of the protons with Na ions. The soaking solutions were then titrated with NaOH with a phenolphthalein indicator to determine the end point. The resulting IEC values are displayed in Table 3.4. The conductivity to IEC ratio varies greatly between the films examined. Films with a higher ratio have higher proton mobilities. TL films assembled with $CaCl_2$ have twice as many free protons as films assembled with Na.

LbL Film	σ_H (mS/cm) at 98%RH	IEC (mmol/g)	σ_H/IEC (mS•g)/(mmol•cm)
PDAC/sPPO (0.75M Ca, pH1)	70	0.44	159
PDAC/sPPO (0.25M Ca, pH1)	4	0.24	17
PDAC/sPPO/PDAC/PEDOT:sPPO (0.25M Ca, pH2)	4	0.15	27
PDAC/sPPO/PDAC/PEDOT:sPPO (0.5M Na, pH2)	*	0.08	*

Table 3.4. Proton exchange capacities of purely ion conducting LbL films and of mixed conducting LbL films. *These values could not be determined due to overlap of features in the impedance spectrum.

3.4 Conclusion

We have generated an array of transparent mixed conducting polymer films with tunable transparency and conductivity properties by incorporating PEDOT:sPPO into LbL films and varying the composition ratio of the film components. The visible light transmission properties are excellent: 1.1 μm thick films with 150 mS/cm electrical conductivity have 80% transmission of light in the visual range. The electronic and ionic conductivities are inversely related, as one can be increased at the expense of the other. We have generated 4.6 μm thick films with 2 mS/cm electrical and 4 mS/cm protonic conductivity; these films surpass the conductivity goals set by the desired future application of these films as membranes for photoelectrochemical cells.

Microscopy studies showed that PEDOT:sPPO preaggregated to form nanofibular structures, and that that these structures can form a percolative network throughout the films, thus providing for electrical conductivity despite the presence of insulating PDAC. Temperature-dependent impedance studies and ion exchange capacity measurements indicated that addition of Ca^{2+} salts provided an increase in ionic conductivity over addition of Na^{+} salts by increasing the number of free protons present in the films, but did not improve the proton mobility of the films.

This series of mixed conducting films with tunable transparency and conductivity properties are promising for many applications such as battery electrodes, chemical sensors, gas separators, wireless photosynthesis devices, and electrochromic windows. Investigations into integrating these films with microstructured photoelectrodes for use as membranes for solar-powered water-splitting devices are ongoing.

3.5 References

1. (a) Maier, J., Nanoionics: ion transport and electrochemical storage in confined systems. *Nature Materials* **2005,** *4* (11), 805-815; (b) Weppner, W., Materials concepts for solid state ionic devices. *Solid State Ionics: Trends in the New Millennium, Proceedings* **2002,** 409-409; (c) Javier, A. E.; Patel, S. N.; Hallinan, D. T.; Srinivasan, V.; Balsara, N. P., Simultaneous Electronic and Ionic Conduction in a Block Copolymer: Application in Lithium Battery Electrodes. *Angewandte Chemie-International Edition* **2011,** *50* (42), 9848-9851; (d) McFarlane, S. L.; Day, B. A.; McEleney, K.; Freund, M. S.; Lewis, N. S., Designing electronic/ionic conducting membranes for artificial photosynthesis. *Energy & Environmental Science* **2011,** *4* (5), 1700-1703; (e) Spurgeon, J. M.; Walter, M. G.; Zhou, J. F.; Kohl, P. A.; Lewis, N. S., Electrical conductivity, ionic conductivity, optical absorption, and gas separation properties of ionically conductive polymer membranes embedded with Si microwire arrays. *Energy & Environmental Science* **2011,** *4* (5), 1772-1780.

2. Haussener, S.; Xiang, C.; Spurgeon, J. M.; Ardo, S.; Lewis, N. S.; Weber, A. Z., Modeling, simulation, and design criteria for photoelectrochemical water-splitting systems. *Energy & Environmental Science* **2012,** *5*, 9922-9935.

3. (a) Granstrom, M.; Inganas, O., Flexible arrays of submicrometer-sized polymeric light emitting diodes. *Advanced Materials* **1995,** *7* (12), 1012-&; (b) DeLongchamp, D.; Hammond, P. T., Layer-by-Layer Assembly of PEDOT/Polyaniline Electrochromic Devices. *Advanced Materials* **2001,** *13* (19), 1455-1459; (c) Nagarajan, S.; Kumar, J.; Bruno, F. F.; Samuelson, L. A.; Nagarajan, R., Biocatalytically synthesized poly(3,4-ethylenedioxythiophene). *Macromolecules* **2008,** *41* (9), 3049-3052; (d) Heywang, G.; Jonas, F., Poly(Alkylenedioxythiophene)S - New, Very Stable Conducting Polymers. *Advanced Materials* **1992,** *4* (2), 116-118.

4. Liu, J.; Davis, N. R.; Liu, D. S.; Hammond, P. T., Highly transparent mixed electron and proton conducting polymer membranes. *Journal of Materials Chemistry* **2012,** *22*, 15534.

5. Ashcraft, J. N.; Argun, A. A.; Hammond, P. T., Structure-property studies of highly conductive layer-by-layer assembled membranes for fuel cell PEM applications. *Journal of Materials Chemistry* **2010,** *20*, 6250-6257.

6. Argun, A. A.; Ashcraft, J. N.; Hammond, P. T., Highly Conductive, Methanol Resistant Polyelectrolyte Multilayers. *Advanced Materials* **2008,** *20*, 1539-1543.

7. (a) Argun, A. A.; Ashcraft, J. N.; Hammond, P. T., Highly conductive, methanol resistant polyelectrolyte multilayers. *Advanced Materials* **2008,** *20* (8), 1539-+; (b) Ashcraft, J. N.; Argun, A. A.; Hammond, P. T., Structure-property studies of highly conductive layer-by-layer assembled membranes for fuel cell PEM applications. *Journal of Materials Chemistry* **2010,** *20* (30), 6250-6257.

8. Dubas, S. T.; Schlenoff, J. B., Factors Controlling the Growth of Polyelectrolyte Multilayers. *Macromolecules* **1999,** *32* (24), 8153-8160.

9. Shiratori, S. S.; Rubner, M. F., pH-Dependent Thickness Behavior of Sequentially Adsorbed Layers of Weak Polyelectrolytes. *Macromolecules* **2000,** *33* (11), 4213-4219.

10. Liu, D. S. Controlling the Mechanical and Transport Properties of Layer-by-Layer Films and Electrospun Mat Composite Membranes for Fuel Cell Applications. Massachusetts Institute of Technology, 2014.

11. Smith, R. R.; Smith, A. P.; Stricker, J. T.; Taylor, B. E.; Durstock, M. F., Layer-by-layer assembly of poly(3,4-ethylenedioxythiophene): Poly(3,4-ethylenedioxythiophene): poly(styrenesulfonate). *Macromolecules* **2006,** *39* (18), 6071-6074.

12. Kim, S. Y.; Hong, J.; Kavian, R.; Lee, S. W.; Hyder, M. N.; Shao-Horn, Y.; Hammond, P. T., Rapid fabrication of thick spray-layer-by-layer carbon nanotube electrodes for high power and energy devices. *Energy & Environmental Science* **2013,** *6* (3), 888-897.

13. Decher, G., Fuzzy Nanoassemblies: Toward Layered Polymeric Multicomposites. *Science* **1997,** *277*, 1232.

14. Orazem, M. E.; Tribollet, B., *Electrochemical Impedance Spectroscopy*. Wiley & Sons: 2008.

15. (a) Ren, X. M.; Pickup, P. G., Ion-Transport in Polypyrrole and a Polypyrrole Polyanion Composite. *Journal of Physical Chemistry* **1993,** *97* (20), 5356-5362; (b) Li, G.; Pickup, P. G., Ion Transport in a Chemically Prepared Polypyrrole/Poly(styrene-4-sulfonate) Composite. *J. Phys. Chem. B* **1999,** *103*, 10143-10148.

16. Ren, X.; Pickup, P. G., Ionic and Electronic Conductivity of Poly-(3-methylpyrrole-4-carboxylic Acid). *J. Electrochem. Soc.* **1992,** *139*, 2097-2105.

17. (a) Huggins, R. A., Simple method to determine electronic and ionic components of the conductivity in mixed conductors a review. *Ionics* **2002,** *8* (3-4), 300-313; (b) Jamnik, J.; Maier, J., Treatment of the Impedance of Mixed Conductors Equivalent Circuit Model and Explicit Approximate Solutions. *J Electrochem Soc* **1999,** *146* (11), 4183-4188.

Appendix A. Other Mixed Conducting LbL Systems

In addition to PEDOT, we examined two other electrically conductive materials combined with sPPO to generate mixed conducting composites: polyaniline (PANI) and amine-functionalized multi-walled carbon nanotubes (MWNT). However, the ionic conductivities of these films have yet to be determined. Impedance spectra of PANI/sPPO in the in-plane configuration displayed one semi-circle with a resistance equivalent to the electrical resistance, and measurements in solution resulted in film delamination.

PANI/sPPO LbL Film Assembly: Films were assembled with an automated ZEISS DS50 slide stainer on glass substrates that were exposed to O_2 plasma for 4 min to induce a negative surface charge. Films were immersed for 15 min. in the polymer solutions (starting with the polycation), followed by immersion for 2 min. each in a series of 3 rinse baths. The PANI bath was stirred throughout the assembly process to provide more uniform film thickness. Surprisingly, while aqueous dispersions of PANI powder built films readily, solutions of PANI nanofibers did not build films with sPPO or with PSS under any conditions, but did build films when paired with polyacrylic acid.

PANI solution: 100 mg polyaniline (emeraldine base, Aldrich 50,000 ave MW) was dissolved in 10 mL dimethylacetamide (DMAc) overnight. The DMAc soln was added to 90 mL of pH 3 water (Milli- Q water, pH adjusted with HCl). The solution was sonicated for 15 min, then the pH was adjusted to 2.5 with HCl. The solution was sonicated for 2 h., filtered through a 0.45 micron nylon membrane, and re-adjusted to pH 2.5.

sPPO solution: 10mM aq. sulfonated poly(2,6-dimethyl 1,4-phenylene oxide) (sPPO) adjusted to pH 2.5 with HCl.

Rinse solution: Deionized water adjusted to pH 2.5 with HCl.

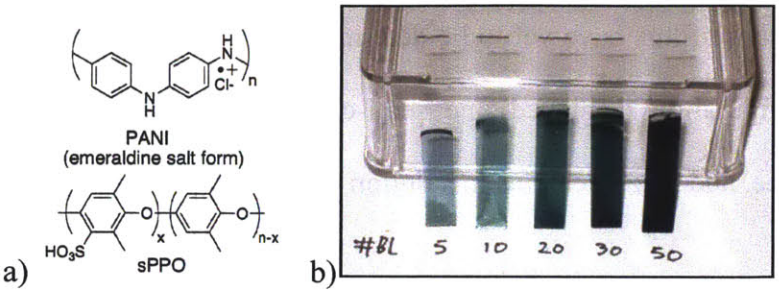

Figure A.1 a) Chemical structures of polyaniline (PANI) and sulfonated polyphenylene oxide (sPPO). **b**) Photograph showing PANI/sPPO films on glass of increasing numbers of bilayers. Electrical conductivity of these films was 0.15 mS/cm initially, but rose to 0.82 mS/cm when doped by exposure to HCl vapor.

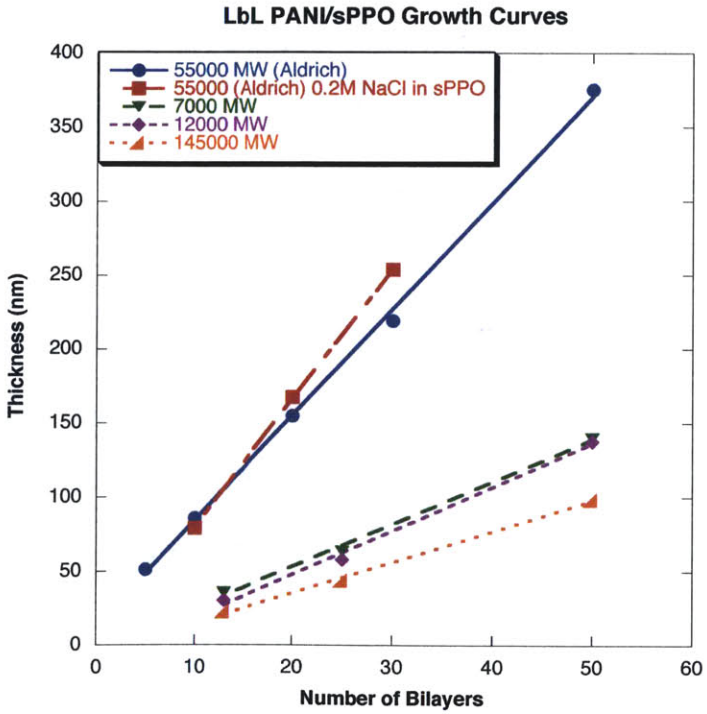

Figure A.2. Growth curves for PANI/sPPO LbL films exhibiting linear growth. Commercially available PANI with a 55,000 MW built the thickest films with a growth rate of 8.7 or 7 nm/BL depending on whether or not salt was added to the sPPO solution. In-house synthesized PANI with both much lower (7,000, 12,000) and much higher (145,000) molecular weights built films at much slower rates of 3 and 2 nm/BL respectively.

a)

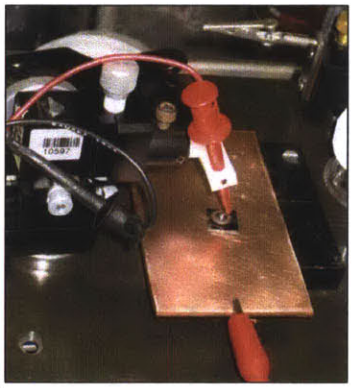

b)

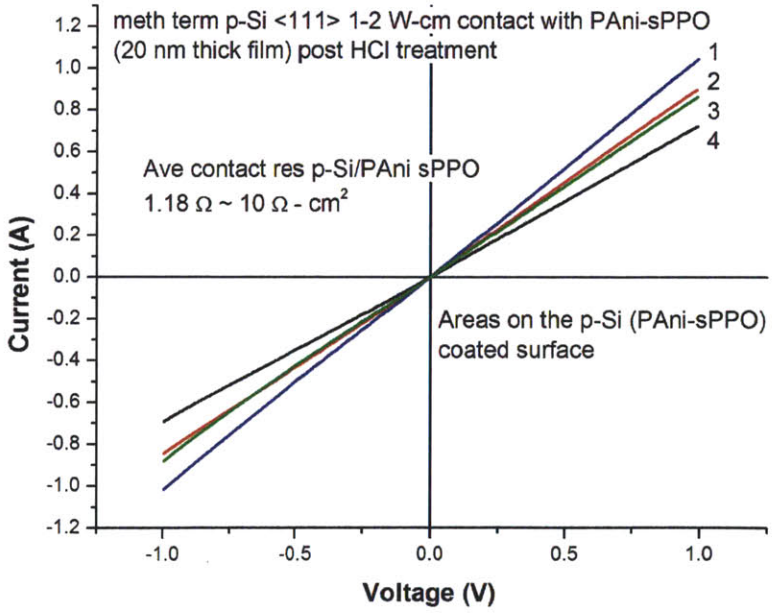

Figure A.3. **a**) PANI/sPPO films were assembled on both H-terminated and methyl-terminated p-doped Si samples. Electrical contact measurements were performed using a gallium/indium amalgam back-contact between the Si and a copper plate, and a mercury drop

top-contact to the LbL film. **b)** PANI/sPPO films made ohmic contacts to methyl-terminated p-Si, but rectifying contacts to H-terminated p-Si. It is possible that the H-terminated Si developed an oxide layer due to oxygen exposure, (creating a barrier to ohmic electrical contacts) either during the LbL dipping process, or after film formation (indicating that the LbL film was not protective of the Si-H surface).

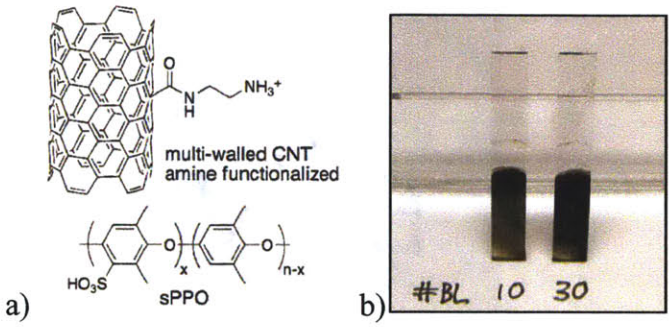

Figure A.4 a) Chemical structures of amine-functionalized multi-walled carbon nanotubes (MWNT) and sPPO. **b)** Photograph showing MWNT/sPPO LbL films on glass. The films are 215 and 580 nm thick for 10 and 30 BL respectively, with electrical conductivity values of 1.37 and 1.91 S/cm. All MWNT LbL films have electrical conductivities of 1–2 S/cm; these similar conductivity values indicate that the MWNTs formed a percolative network in the sPPO films. The films were prepared in a similar manner as the PANI/sPPO films described above, and the MWNT solution was prepared according to this reference: Lee, S. W.; Kim, B.; Chen, S.; Shao-Horn, Y.; Hammond, P. T. *J. Am. Chem. Soc.* **2009**, *131*, 671.

Appendix B. Efforts Towards a Model Device

In order to generate a model device, the mixed conducting materials from Chapter 3 must be combined with the fabrication methods of Chapter 2. Preliminary efforts toward this are described in the following figures.

Transfer printing of mixed conducting films:
σ_e= 40 mS/cm
σ_H= 0.013 mS/cm

Figure B.1. Multilayer transfer printing of a tetralayer film demonstrated that electrical conductivity was preserved across the merged interface.

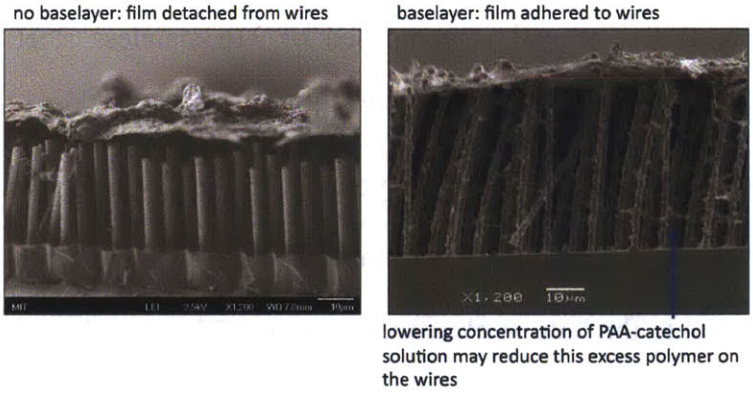

Figure B.2. Dip-LbL assembly of PDAC/sPPO BL LbL films on methyl-terminated silicon microwires resulted in bridging films, but the film did not adhere well to the substrate. Use of a catechol-modified PAA baselayer improves adhesion.

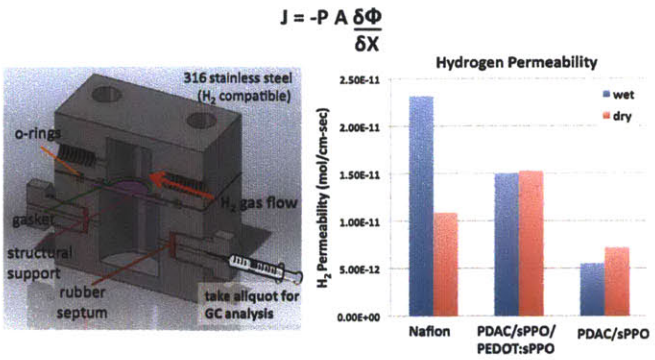

Figure B.3. a) Schematic of cell designed for measuring hydrogen permeability. **b**) Hydrogen permeability of PEDOT:sPPO TL films was roughly the same as the permeability of Nafion, whereas PDAC/sPPO permeability was half as much.

The hydrogen permeability of commercial Nafion films and of ultrathin LbL films built on track-etched polycarbonate membranes was measured using a custom-designed cell illustrated in Figure B.3. The cell is composed of 316 stainless steel because it is H_2 compatible, and the cell was shown capable of holding up to 5 atm. of H_2 pressure without leaking. The cell consists of a top chamber (volume 2.75 cm^3) through which either dry or humidified to 50 % relative humidity H_2 was pushed at a flow rate of 200 mL/min. This top chamber is tightened onto the bottom chamber (volume 7.78 cm^3) with 4 screws. In between the two chambers sits a gasket and two sets of o-rings on top of the membrane to be measured and a porous support. The area if the hole in the gasket (and hence the active membrane area for these experiments) was 1.13 cm^3. While H_2 flowed through the top chamber, 250 μL aliquots of gas were removed at regular intervals from the bottom chamber and injected into a gas chromatograph with a thermal conductivity detector to measure the hydrogen concentration. The hydrogen crossover with respect to time was used to calculate a flux, which was used to calculate the permeability according to the equation shown in Figure B.3.

Chapter 4.

Conclusions and Recommendations for Future Work

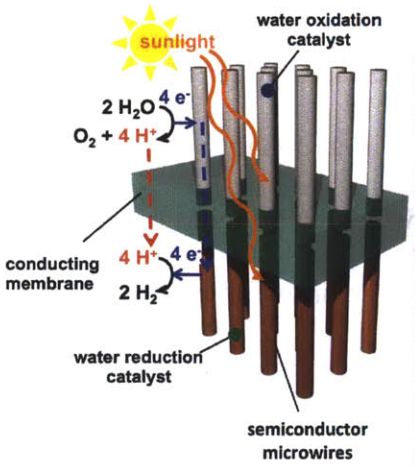

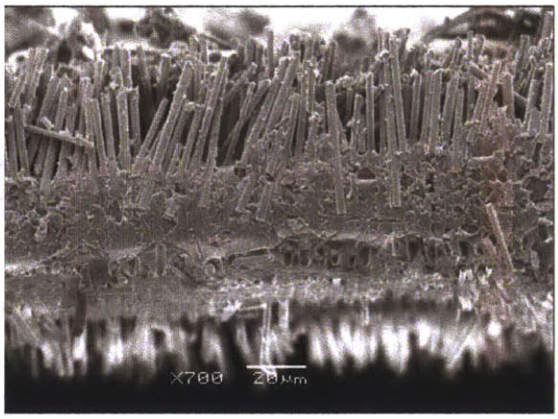

4.1 Thesis Conclusions

The objectives of this thesis were to develop materials and fabrication methods that could be used to generate transparent mixed conducting membranes and to integrate them with microstructured electrodes for photoelectrochemical cells. Great progress made on each of these goals, and the combination of the new materials with the new fabrication methods was begun.

4.1.1 Fabrication of Membrane Electrode Assemblies

Fabrication methods to incorporate LbL films with silicon microwires in a controlled fashion were studied with two ion conducting LbL systems, PDAC/sPPO and LPEI/PAA. The choice of LbL assembly platform, Dip- or Spray-LbL, was found to influence whether film coverage was conformal around the length of the wires, or bridging across the top of the array. The controlling factors for the film location on the arrays were identified, as were the boundaries of when control switches from one factor to another. Silicon surface chemistry was the main controlling factor of film coating location when the surface was hydrophobic (water contact angle greater than 90° on planar Si): bridging films around the top 5 μm of the array were formed with both Dip- and Spray-LbL. For silicon surface chemistries with water contact angles below 90°, the polymer spray time and the wire array spacing were found to be the determinant factors. The polymer spray time influenced the penetration depth of bridging films by transferring the momentum of the arriving droplets onto the capillary bridge, pushing the bridge deeper into the array. For wire spacing below or equal to the 10 μm droplet size, Spray-LbL formed bridging films. With wire spacing greater than 10 μm, Spray-LbL formed conformal coatings along the length of the wires until the spacing was narrowed by the

increased diameter of the coated wires, at which point bridging behavior began to be observed.

Spray-LbL assembly was used to embed and transfer vertically aligned Si microwire arrays into free-standing ion-conducting functional membranes. This fabrication method was shown to be modular: two free-standing membrane-microwire assemblies were merged into a single functional film, demonstrating the extension of multilayer assembly and transfer to 3-D microfabrication. This technique appears to be general and could be extended to other types of functional LbL films, such as electrically or mixed conductive films, as well as films with tunable permeability to molecules, enabling the assembly of complex devices that could be adapted to mediate transport between active components. The ability to control the thickness of the film, to fine tune its composition along the *z*-direction, and to limit film formation to specific regions of the wire array on the micron-scale are attractive features of this method that distinguish it from the use of bulk polymers. Ultimately, this set of approaches could offer options relative to traditional materials for microfabrication of Si devices such as solar-driven water splitting systems, capacitors, or electrochemically active electrodes.

4.1.2 Mixed Conducting Materials With Tunable Properties

We generated a series of transparent mixed conducting polymer films with tunable transparency and conductivity properties by incorporating PEDOT:sPPO into LbL films and varying the composition ratio of the film components. Films that met the desired criteria for use as a membrane in solar-powered water-splitting devices were generated. The visible light transmission properties were excellent: 1.1 μm thick films with 150 mS/cm electrical conductivity had 80% transmission of light in the visual range. The electronic and ionic

conductivities were found to be inversely related, as one could be increased at the expense of the other. Films with nearly equal electrical and ionic conductivity values were assembled: 4.6 μm thick films with 2 mS/cm electrical and 4 mS/cm protonic conductivity. These films surpass the conductivity goals set by the desired future application of these films as membranes for photoelectrochemical cells.

The composition percentage of sPPO in the films was increased by building films with a tetralayer architecture, and were increased further through increased charge shielding by adding divalent salts to the sPPO assembly bath. Microscopy studies showed that PEDOT:sPPO pre-aggregated to form nanofibular structures, and that that these structures can form a percolative network throughout the films, thus providing for electrical conductivity despite the presence of insulating PDAC. Temperature-dependent impedance studies and ion exchange capacity measurements indicated that addition of Ca^{2+} salts provided an increase in ionic conductivity over addition of Na^{+} salts by increasing the number of free protons present in the films, but did not improve the proton mobility of the films.

This series of mixed conducting films with tunable transparency and conductivity properties are promising for many applications such as battery electrodes, chemical sensors, gas separators, wireless photosynthesis devices, and electrochromic windows.

4.2 Unanswered Questions & Recommendations for Future Work

The next goals for this project are to generate a merged structure of two membrane-microwire electrode assemblies, to test the conductivity and H_2/O_2 permeability properties of this model device, and eventually to use this model device in a photoelectrochemical cell,

such as one that splits HBr (which is easier than testing water-splitting). Some challenges and questions remain before this can be accomplished.

The conductivity values of some of the mixed conducting PEDOT:sPPO LbL films are high enough for the films to be useful in a working device, but the other factor that controls whether the voltage losses through the will be in an acceptable range is the electrical contact between the membrane and the semiconductor photoelectrodes. The contact between PEDOT:PSS and PEDOT/Nafion mixtures has been examined in detail, but only preliminary studies of the electrical contact between Si and PEDOT:sPPO LbL films have been completed.

The mechanical properties of the PEDOT:sPPO LbL films remain to be explored. Whether they can support an array of Si microwires in both the wet and dry state will be an important parameter to understand. The mechanical strength of the bond between merged films should also be investigated. Understanding this parameter and how it is affected by the mechanical properties of the unmerged LbL system will be an important step in generalizing the use of merged LbL films as conductive glue.

The conductivity values and the most representative equivalent circuit model for the impedance of PEDOT:sPPO-containing LbL films remain to be clarified. Our recommendation to accomplish this is to re-measure the impedance of this series of films in a different cell with much smaller and more carefully controlled distances between the electrodes. Alternatively, it might be preferable to eliminate the use of solution entirely and to instead use a metallic top contact for the surface of the films such as coating them with evaporated gold.

Further research into improving the electrical properties of sprayed PEDOT:sPPO LbL films is also warranted. Spray-LbL is dramatically faster than Dip-LbL, for instance assembling 100 BL requires 1 h by spraying, or 3 days if dipping. In order to eventually produce these materials economically, speeding up the process will be required.

Alternate device designs for the solar water-splitting device are also worth exploring. The Si microwires intended for use as the photocathode in the current device design cannot be used in the harshly oxidizing environment of the photoanode without some sort of protective coating to prevent oxidation. An alternate photoanode design involves generating an LbL carbon nanotube nanostructured network containing catalyst nanoparticles, which could be built directly onto an LbL membrane-Si microwire electrode assembly (Figure 4.1).

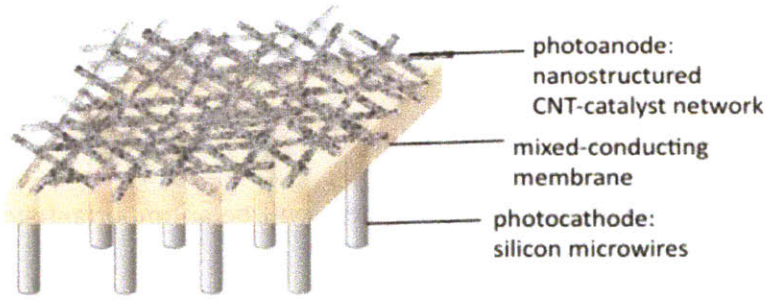

Figure 4.1. Proposed device design consisting of a Si microwire photocathode, an LbL film mixed conducting membrane, and an LbL carbon nanotube photoanode.